$Ca_V2.1$ α_1 subunit motifs that control presynaptic $Ca_V2.1$ subtype abundance are distinct from $Ca_V2.1$ preference

Jianing Li[1,2], Priyadharishini Veeraraghavan[1], Samuel M. Young, Jr[1,3^]

[1]Department of Anatomy and Cell Biology, University of Iowa, Iowa City, IA, USA.
[2]Cell Developmental Biology Graduate Program, University of Iowa, Iowa City, IA 52242, USA
[3]Department of Otolaryngology, Iowa Neuroscience Institute, University of Iowa, Iowa City, IA, USA.

^Correspondence
Samuel M. Young, Jr. PhD
Department of Anatomy and Cell Biology
University of Iowa
PBDB 5322
169 Newton Road
Iowa City, IA 52242
Email: samuel-m-young@uiowa.edu

ORCIDs:

Jianing Li	0000-0001-5384-773X
Priyadharishini Veeraraghavan	0000-0003-2826-1686
Samuel M. Young, Jr.	0000-0002-7589-7612

Key points summary:

- Presynaptic Ca_V2 subtype abundance regulates neuronal circuit properties, however the mechanisms regulating presynaptic Ca_V2 subtype abundance and preference remains enigmatic.
- The Ca_V α_1 subunit determines subtype and contains multiple motifs implicated in regulating presynaptic subtype abundance and preference.
- The $Ca_V2.1$ α_1 subunit domain II-III loop and cytoplasmic C-terminus are positive regulators of presynaptic $Ca_V2.1$ abundance but do not regulate preference.
- The $Ca_V2.3$ α_1 subunit cytoplasmic C-terminus negatively regulates presynaptic Ca_V2 subtype abundance but not preference while the $Ca_V2.2$ α_1 subunit cytoplasmic C-terminus is not a key regulator of presynaptic Ca_V2 subtype abundance or preference.
- The Ca_V2 α_1 subunit motifs determining the presynaptic Ca_V2 preference are distinct from abundance.

Abstract

Presynaptic voltage-gated Ca^{2+} channels (Ca_V) subtype abundance at mammalian synapses regulates synaptic transmission in health and disease. In the mammalian central nervous system, most presynaptic terminals are $Ca_V2.1$ dominant with a developmental reduction in $Ca_V2.2$ and $Ca_V2.3$ levels, and Ca_V2 subtype levels are altered in various diseases. However, the molecular mechanisms controlling presynaptic Ca_V2 subtype levels are largely unsolved. Since the Ca_V2 α_1 subunit cytoplasmic regions contain varying levels of sequence conservation, these regions are proposed to control presynaptic Ca_V2 subtype preference and abundance. To investigate the potential role of these regions, we expressed chimeric $Ca_V2.1$ α_1 subunits containing swapped motifs with the $Ca_V2.2$ and $Ca_V2.3$ α_1 subunit on a $Ca_V2.1/Ca_V2.2$ null background at the calyx of Held presynaptic terminal. We found that expression of $Ca_V2.1$ α_1 subunit chimeras containing the $Ca_V2.3$ loop II-III region or cytoplasmic C-terminus (CT) resulted in a large reduction of presynaptic Ca^{2+} currents compared to the $Ca_V2.1$ α_1 subunit. However, the Ca^{2+} current sensitivity to the $Ca_V2.1$ blocker Agatoxin-IVA, was the same between the chimeras and the $Ca_V2.1$ α_1 subunit. Additionally, we found no reduction in presynaptic Ca^{2+} currents with $Ca_V2.1/2.2$ cytoplasmic CT chimeras. We conclude that the motifs in the $Ca_V2.1$ loop II-III and CT do not individually regulate $Ca_V2.1$ preference, but these motifs control $Ca_V2.1$ levels and the $Ca_V2.3$ CT contains motifs that negatively regulate presynaptic $Ca_V2.3$ levels. We propose that the motifs controlling presynaptic $Ca_V2.1$ preference are distinct from those regulating $Ca_V2.1$ levels and may act synergistically to impact pathways regulating $Ca_V2.1$ preference and abundance.

61 **Introduction**

62 At mammalian central nervous system (CNS) synapses, $Ca_V2.1$, $Ca_V2.2$, and $Ca_V2.3$, are
63 key determinants of Ca^{2+} entry that controls synaptic transmission and neuronal circuit function
64 (Dolphin & Lee, 2020; Young & Veeraraghavan, 2021). Among the three Ca_V2 subtypes,
65 presynaptic $Ca_V2.1$ levels are dominant compared to $Ca_V2.2$ and $Ca_V2.3$ (Iwasaki & Takahashi,
66 1998; Iwasaki *et al.*, 2000; Nanou & Catterall, 2018; Dolphin & Lee, 2020). During neuronal circuit
67 maturation, action-potential (AP) evoked synaptic transmission becomes increasingly $Ca_V2.1$-
68 dependent due to a selective presynaptic reduction of $Ca_V2.2$ and $Ca_V2.3$ (Iwasaki & Takahashi,
69 1998; Eggermann *et al.*, 2011; Young & Veeraraghavan, 2021). In addition, presynaptic Ca_V2
70 subtype levels vary between synapses and are altered in various diseases (Dolphin & Lee, 2020;
71 Young & Veeraraghavan, 2021). Since Ca_V2 subtypes differentially control Ca^{2+} influx, elucidating
72 the molecular mechanisms controlling presynaptic Ca_V2 subtype abundance are critical to
73 understanding brain function in health and disease.

74 Although presynaptic Ca_V2 subtype levels are highly variable, they are distinct between the
75 neuronal soma and presynaptic terminal (Doughty *et al.*, 1998). In addition, loss of $Ca_V2.1$ leads
76 to increases in presynaptic $Ca_V2.2$ levels, however total presynaptic Ca^{2+} currents are reduced
77 (Jun *et al.*, 1999; Inchauspe *et al.*, 2004; Lubbert *et al.*, 2017). Therefore, it is proposed that
78 mechanisms that control presynaptic Ca_V2 levels and preferences are distinct from those
79 controlling somatic Ca_V2 levels (Weiss & Zamponi, 2017; Dolphin & Lee, 2020). However, whether
80 the mechanisms that determine presynaptic Ca_V2 subtype preference and abundance are
81 interrelated or separable are unknown.

82 The pore- forming Ca_V2 α_1 subunit determines presynaptic Ca_V2 preference and contains
83 multiple cytoplasmic protein interaction motifs (Dolphin & Lee, 2020). Due to varying levels of
84 sequence conservation between the three Ca_V2 α_1 subunit isoforms cytoplasmic regions, three
85 regions are implicated in regulating presynaptic Ca_V2 channel levels. They are: 1) the I-II loop;
86 the primary binding site to the $Ca_V\beta$ subunit (AID) 2) the II-III loop; the synprint domain; and 3)

87 the C-terminal region, which contains multiple active zone (AZ) protein binding sites and is
88 frequently mutated in Ca_V2 channelopathies (Dolphin & Lee, 2020; Young & Veeraraghavan,
89 2021). Since the loop II-III and cytoplasmic CT regions are not highly conserved between the
90 different Ca_V2 α_1 subunit isoforms and are subject to alternative splicing (Simms, 2014), they are
91 speculated to contain motifs that regulate the presynaptic Ca_V2 subtypes levels and preference.
92 However, the identity of the Ca_V2 α_1 subunit motifs that regulate presynaptic Ca_V2 subtype levels
93 and preference is unclear. Studies from cultured superior cervical ganglion neurons demonstrated
94 that the $Ca_V2.1$ loop II-III domain regulates presynaptic targeting (Mochida *et al.*, 2003). However,
95 it is not defined if the $Ca_V2.1$ loop II-III region is a key determinant of preference or if the II-III
96 region from other Ca_V2 subtypes regulates abundance and preference. Although motifs in the
97 $Ca_V2.1$ CT (aa. 2016-2368) that interact with AZ proteins are dispensable for controlling
98 presynaptic $Ca_V2.1$ abundance (Lubbert *et al.*, 2017), it is not known if other regions in the $Ca_V2.1$
99 CT control Ca_V2 subtype abundance and preference. Furthermore, whether the $Ca_V2.2$ and
100 $Ca_V2.3$ CT regulates abundance and preference is unresolved.

101 To elucidate the roles of the Ca_V2 α_1 subunit loop II-III and CT in regulating presynaptic
102 abundance and preference in a native neuronal circuit, we generated Ca_V2 α_1 subunit chimeras:
103 1) <u>$Ca_V2.1/2.3$ chimeras</u>, the $Ca_V2.1$ α_1 subunit II-III loop and/or CT region, were swapped with
104 these regions from the $Ca_V2.3$ α_1 subunit. 2) <u>$Ca_V2.1/2.2$ chimeras,</u> $Ca_V2.1$ α_1 subunit CT region
105 was swapped with the $Ca_V2.2$ α_1 subunit CT region. We then used helper-dependent Adenoviral
106 (HdAd) technology and delivery techniques to express $Ca_V2.1$ α_1 subunit chimeras on a
107 $Ca_V2.1/Ca_V2.2$ null background at the postnatal days (P) 9–11 calyx of Held using a
108 *Cacna1a*/*Cacna1b flox/flox* ($Ca_V2.1$ $Ca_V2.2$ CKO) mouse model. The calyx of Held is a large
109 glutamatergic presynaptic terminal in the auditory brainstem that at this developmental stage
110 contains multiple Ca_V2 subtypes which is similar to the majority of presynaptic terminals (Iwasaki
111 *et al.*, 2000; Young & Veeraraghavan, 2021).

112 Using direct presynaptic Ca^{2+} current recordings at the calyx of Held, we found that
113 ablation of $Ca_V2.1$ and $Ca_V2.2$ resulted in a significant reduction in total presynaptic Ca^{2+} currents
114 and were insensitive ω-Agatoxin-IVA (Aga), a $Ca_V2.1$ specific blocker, and ω-Conotoxin GVIA
115 (Cono), a $Ca_V2.2$ specific blocker, and Nifedipine a Ca_V1 specific blocker, but were partially
116 sensitive to SNX-482, a $Ca_V2.3$ specific blocker. Expression of $Ca_V2.1/2.3$ chimeras with single
117 or combined region swaps resulted in a significant reduction in peak Ca^{2+} current amplitudes.
118 However, the remaining Ca^{2+} currents with the single swap $Ca_V2.1/2.3$ chimeras exhibited a
119 similar proportion of Aga sensitive currents as the full transcript (FT) $Ca_V2.1$ α_1 subunit, while the
120 combined swap had a significant increase in Aga insensitive Ca^{2+} currents. In addition, expression
121 of $Ca_V2.1/2.3$ chimeras which replaced the dispensable region of the $Ca_V2.1$ CT (aa. 2016-2368)
122 with corresponding $Ca_V2.3$ CT region resulted in a reduction in Ca^{2+} currents. Finally, we found
123 that expression of $Ca_V2.1/2.2$ CT chimeras revealed no reduction in presynaptic Ca^{2+} currents.
124 Based on our data, we conclude that individual motifs in the $Ca_V2.1$ α_1 subunit loop II-III
125 or CT are positive regulators of presynaptic $Ca_V2.1$ levels but do not individually control $Ca_V2.1$
126 preference. Furthermore, we conclude the $Ca_V2.3$ CT contains motifs that negatively regulate
127 presynaptic $Ca_V2.3$ levels. Therefore, we propose that the motifs that determine presynaptic
128 $Ca_V2.1$ abundance are distinct from those regulating $Ca_V2.1$ preference and these motifs may
129 synergistically impact pathways that regulate $Ca_V2.1$ preference and levels.

Methods and materials

Ethical approval

All procedures were performed according to the animal welfare law of the University of Iowa Office of Animal Resources (OAR) and Institutional Animals Care and Use Committee (IACUC, D16-00009 (A3021-01)). Mice are maintained at The University of Iowa Animal Care Facility which is approved under NIH assurance A3021-01 and certified by the State of Iowa for use of living animals. Animals were housed with 12 h light/dark cycle and *ab libitum* food/water supply. Animals of both sexes at postnatal day 9-11 were used for all experiments. All available measures were taken to minimize animal pain and suffering.

EXPERIMENTAL DESIGN

Generation of *Cacna1a*/*Cacna1b* flox/flox animal

Cacna1a fl/fl mice

Cacna1a$^{fl/fl}$ mice were generated as follows. The Cacna1a$^{tm1a(EUCOMM)Hmgu}$ targeting vector (EUMMCR) was electroporated into the JM8A3 ES-cells derived from C57BL/6N mice and clones were selected and PCR verified. The neo gene was removed by crossing to FLPo mice carrying the FLP recombinase gene under the control of the CAG promoter (C57BL/6N-Tg (CAG-Flpo)1Afst/Mmucd, stock 036512-UCD. (Mouse Biology Program KOMP). Genotyping of *Cacna1a* flox mice by PCR was carried out by the following primers,

754 5' GGAATCCCAAGTGCGTGAGTCTCC 3'

887 5' TCAGCCCCTTCTCTTTAATCTGACCC 3'

Cacna1a$^{fl/fl}$ mice were backcrossed to C57BL6/J background.

Cacna1b$^{fl/fl}$ *mice*

Cacna1b$^{fl/fl}$ *mice* (*C*57BL/6N-Cacna1b$^{tm1c(KOMP)Wtsi}$/H) were purchased from MRC Harwell Institute. Genotyping of *Cacna1b*$^{fl/fl}$ was carried out using the following primers,

Cacna1b-5arm-WTF 5' TTGGTGTCCTGTTCTCCACA 3'

Cacna1b-Crit-WTR 5' CAGGGAATCCTGGGAAGTAA 3'

156 **5mut-R1** 5' GAACTTCGGAATAGGAACTTCG 3'

157 *Cacna1b*$^{fl/fl}$ *mice* were backcrossed to the C57BL6/J background.

158 *Cacna1a*$^{fl/fl}$*, Cacna1b*$^{fl/fl}$ mice

159 *Cacna1a*$^{fl/fl}$*, Cacna1b*$^{fl/fl}$ mice were generated by crossbreeding *Cacna1a*$^{fl/fl}$ with *Cacna1b*$^{fl/fl}$ to

160 homozygosity. Genotyping was performed by PCR.

161 **Stereotactic P1 surgery**

162 Stereotactic surgery was performed at P1 as described previously (Radulovic *et al.*, 2020). Briefly,

163 *Cacna1a*$^{fl/fl}$, *Cacna1b*$^{fl/fl}$ mice were anesthetized by hypothermia, using ice bath for 5min.

164 Subsequently, ~2 µl HdAd in storage buffer (in Mm: 10 HEPES, 250 sucrose, 1 $MgCl_2$ at pH: 7.4

165 and 6.6% mannitol) was injected at 1 µl/min into the cochlear nucleus (CN) using pulled glass

166 pipettes with a 20 µm opening (Sutter Instrument, P-97, U.S.A.). Two viral vectors, expressing

167 Cre and Ca_V2 α_1 hybrid constructs were co-injected. The total viral particle delivered did not

168 exceed $2*10^9$ viral particles. To dissipate pressure after injection, the needle was slowly removed.

169 Animals were then placed under a warming lamp. Upon full recovery, visual inspection and tail

170 pinch responsiveness, animals were returned to their respective cage with the dam. If animals did

171 not recover from the surgery, they were immediately euthanized. In the case of runting or if

172 animals were found in distress at later time points the veterinary staff was consulted and their

173 recommendation for further action was followed.

174 **DNA constructs and recombinant viral vector production**

175 **$Ca_V2.1$ chimeras**

176 Codon optimized (GENEart) $Ca_V2.1$ α_1 subunit cDNA Cacna1a (*Mus musculus*, Accession No.

177 NP_031604.3), $Ca_V2.2$ α_1 subunit cDNA Cacna1b (*Mus musculus,* Accession No.

178 NP_001035993.1) and $Ca_V2.3$ α_1 subunit cDNA Cacna1e (*Mus musculus*, Accession No.

179 NP_033912.2) were used to generate Ca_V2 α_1 hybrid constructs. All Ca_V2 hybrid constructs were

180 sequenced verified. Amino acid alignment of above constructs were were performed under Clustal

181 Omega function using the MegAlign Pro 17 program implemented in the Lasergene software
182 package (v.17, DNASTAR).The following Ca_V2 hybrid constructs were created.
183 $Ca_V2.1/2.3$ II-III loop: $Ca_V2.1$ α_1 subunit aa. 719-1210 replaced with $Ca_V2.3$ α_1 subunit aa. 707-
184 1151
185 $Ca_V2.1/2.3$ CT: $Ca_V2.1$ α_1 subunit aa. 1933-2368 replaced with $Ca_V2.3$ α_1 subunit aa. 1897-2273
186 $Ca_V2.1/2.3$ II-III loop CT: $Ca_V2.1$ α_1 subunit aa. 719-1210 replaced with $Ca_V2.3$ α_1 subunit aa. 707-
187 1151 and $Ca_V2.1$ α_1 subunit aa. 1933-2368 replaced with $Ca_V2.3$ α_1 subunit aa. 1897-2273
188 $Ca_V2.1/2.2$ CT: $Ca_V2.1$ α_1 subunit aa. 1933-2368 replaced by $Ca_V2.2$ α_1 subunit aa. 1870-2327
189 $Ca_V2.1/2.3$ CT1: $Ca_V2.1$ α_1 subunit aa. 2016-2368 replaced with $Ca_V2.3$ α_1 subunit 1952-2273
190 $Ca_V2.1/2.3$ CT2: $Ca_V2.1$ α_1 subunit aa. 1967-2368 replaced by $Ca_V2.3$ α_1 subunit 1929-2273
191 These constructs were individually cloned into the EcoRI and NotI sites of the 470 bp human
192 synapsin (hSyn) neurospecific expression cassette (Montesinos *et al.*, 2016; Dong *et al.*, 2018).
193 **HdAd production**
194 Helper-dependent Adenoviral vector (HdAd) (Cre) which co-expresses Cre recombinase (Cre and
195 EGFP or mCherry under separate neurospecific expression cassettes driven by the 470 bp
196 human synapsin promoter (hSyn) was produced as previously described (Montesinos *et al.*, 2016;
197 Dong *et al.*, 2018). To produce HdAd Ca_V2 chimeric viruses we followed standard protocols
198 (Montesinos *et al.*, 2016; Lubbert *et al.*, 2017). Briefly, Ca_V2 α_1 chimera cDNA constructs driven
199 by hSyn promoter expression casseete or a high-level overexpression pUNISHER (Pun) cassette
200 were then cloned into he AscI site, pdelta23E4 which contains a separate neuro-specific
201 expression of mCherry or myristolated EGFP (mEGFP) markers (Montesinos *et al.*, 2011).
202 Production of HdAd was carried out as previously described (Palmer & Ng, 2005; Montesinos *et*
203 *al.*, 2016). The HdAd plasmid was linearized with PmeI and then transfected (Profection
204 Mammalian Transfection System, Promega, Madison, WI, USA) into 116 producer cells. Helper
205 virus (HV) was added the following day. Forty-eight hours post infection, cells were subjected to
206 three freeze/thaw cycles and lysate was collected. The HdAd vectors were amplified for total of

207 five serial coinfections from 3x6 cm tissue culture dishes followed by one 15 cm dish and finally
208 30x15 cm dishes of 116 cells (confluence ~90%). HdAd was purified by CsCl ultracentrifugation.
209 HdAd was stored at -80°C in storage buffer (10 mM Hepes, 1 mM $MgCl_2$, 250 mM Sucrose, pH
210 7.4).

211 **HdAd titering and quality control**

212 HdAds were titered by qPCR as described previously (Lubbert *et al.*, 2019). The purified reference
213 virus (RV); Ad5-CMV-EGFP (UNC, Gene Therapy Center, Chapel Hill, North Carolina) was titered
214 by endpoint dilution and by transducing units, as described previously (Bewig & Schmidt, 2000).
215 Human Adenovirus 5 Reference Material (ARM), (ATCC, VR-1516). To titer the HdAd by qPCR,
216 adenoviral gDNA from HdAd, RV and ARM was purified from 6 cm plates. Plates were seeded
217 with 3.75 x 10^6 HEK293 cells in DMEM with 10% FBS and coinfected with HdAd plus RV on the
218 following day at a multiplicity of 100 vp/cell. The cells were incubated for 1 hr at 37°C with 5%
219 CO_2 and washed to remove unabsorbed virions. Cells were harvested 4 hr post-infection, then
220 washed with 1 mL PBS and centrifuged for 5 min at 4°C. Pellets were resuspended in 100 mM
221 Tris-HCl, pH 8, lysed by freeze/thaw cycles and treated with 20 U/mL Benzonase for 10 min.
222 Subsequently, lysate was incubated in Proteinase K-SDS solution for 3 hr at 50°C. After protein
223 precipitation with 1.65 M NaCl on ice, DNA was precipitated from supernatants with isopropanol
224 and 3 M sodium acetate, pH 5.2. Samples were mixed well and incubated for 1 hr at -80°C then
225 spun at 4°C for 30 min. Pellets were washed with cold ethanol, dried and resuspended in 10 mM
226 Tris-Cl, pH 8.0. A plasmid standard containing three specific DNA sequences; Ad5 E1a
227 (replication-competent Adenovirus (RCA) detection), Ad5 E2B Iva2 (viral DNA polymerase and
228 terminal protein precursor, HV-exclusive), and Ad genomic stuffer sequence (Cosmid 346 and
229 HPRT1 gene, in all HdAd-exclusive) was used. Three specific primer/probe sets were used for
230 these 3 regions in the plasmid for the detection in qPCR:

231 1.) **Ad5 E1a (RCA):** probe: NED-5'-AGCACCCCGGGCACGGTTG-3'-MGBNFQ; fwd: 5'-
232 GGGTGAGGAGTTTGTGTTAGATTATG-3'; rev: 5'-TCCTCCGGTGATAATGACAAGA-3'

233 2.) **E2B Iva2 (HV):** probe: FAM-5'-TGTCTTTCAGTAGCAAGCT-3'-TAMRA, HV fwd primer:
234 5'-TGGGCGTGGTGCCTAAAA-3', rev: 5'-GCCTGCCCCTGGCAAT-3'
235 3.) **Genomic stuffer DNA (HdAd):** probe: VIC-5'- AGCCTCTCTCATCTCACAGT -3'-
236 MGBNFQ, fwd: 5'-CCCCGCTACCCCAATCC-3', rev: 5'-
237 TTAGCTTTTTTGGGTGATTTTTCC-3'.

238 Sample DNA was diluted 1:10^3, 1:10^4 or 10^5 in 10 mM Tris-Cl, pH 8.0. For HdAd and HV probes,
239 a 6-point standard curve was constructed with the plasmid standard using 10^7- 10^2
240 molecules/well. For RCA detection, two 7-point curves were constructed with 10^7 - 10
241 molecules/well (one plasmid standard and one using ARM gDNA spiked with 10^7 copies of HdAd
242 gDNA). Real-Time PCR parameters were 50°C for 2 min, 95°C for 10 min; 40 cycles of: 95°C for
243 15 sec, 60°C for 1 min. Outliers and results out of range of standard curve were discarded. Results
244 within range of the standard curve were corrected for their dilution and determined as HdAd vector
245 genomes/mL. All samples were negative for RCA.

246 To determine the IU copies/mL from purified coinfection samples, averaged results were
247 divided by 3 µL and multiplied by 25 µL giving IU copies/coinfection. Next, this number was divided
248 by the volume in µL of HdAd added to the coinfection giving IU copies/µL then multiplied by 1000
249 to obtain the i,nfectious HdAd genomes/mL.

250 Calculation to determine the titer of purified HdAd virus:

251 $$HdAd\ infectivity = RV\ infectivity * \frac{HdAd\ vector\ genomes/RV\ genomes}{infectious\ HdAd\ genomes/infectious\ RV\ genomes}$$

252 where Ad5-CMV-EGFP is RV, RV infectivity is VP/IU. IU is the average titer of end point dilution
253 and transducing unit assays, HdAd vector genomes and RV genomes are the number of genomes
254 from purified virus as determined by qPCR, and infectious HdAd genomes and infectious RV
255 genomes are the number of genomes in DNA purified from coinfections. The titers of HdAds carry
256 different cDNA constructs are listed as follow, viral particle/ml: Cre EGFP, 1.75*10^{12}, Cre
257 mCherry, 2.41*10^{12}, syn $Ca_V2.1$ FT, 2.40*10^{12}, Pun $Ca_V2.1$ FT, 2.19*10^{12}, $Ca_V2.1/2.3$ II-III loop

258 CT, 2.00*10^{12}, Ca_V2.1/2.3 II-III loop, 2.07*10^{12}, Syn Ca_V2.1/2.3 CT, 1.90*10^{12}, Pun Ca_V2.1/2.3 CT,
259 3.11*10^{12}, Ca_V2.1 delta 2016, 1.40*10^{12}, Ca_V2.1/2.3 CT 2016-2368, 4.70*10^{12}, Ca_V2.1/2.3 CT
260 1967-2368, 3.29*10^{12}, syn Ca_V2.1/2.2 CT, 3.17*10^{12}, Pun Ca_V2.1/2.2 CT, 9.52*10^{12}. Particle to
261 infectious unit ratio was 10:1~ 50:1. Either syn Cre syn EGFP or syn Cre syn mCherry was used
262 to make sure that the viruses expressing Cre carry different fluorescent protein than the viruses
263 expressing Ca_V2 constructs.

264 **Western Blot**

265 To determine expression of our Ca_V2.1 chimeric constructs, we performed Western Blot
266 analysis on HEK293 cells transduced with our HdAd vectors expressing the Ca_V2 α_1 chimeric
267 constructs. To do so, HEK293 cells were infected with our HdAd vectors, and 48 hrs later cells
268 were collected and lysed in RIPA buffer containing: 10 mM Tris-Cl pH8.0, 1mM EDTA, 1% Triton-
269 X, 0.1% sodium deoxycholate, 0.1% SDS, 140 mM NaCl, protease inhibitor (11836153001,
270 Roche). 20 µg of protein lysate were loaded and analyzed by SDS-PAGE followed by
271 immunoblotting: Ca_V2.1 α_1 CT antibody (Synaptic Systems, #152 203, rabbit polyclonal) diluted
272 1:1000 (final concentration 2 µg/ml) and Ca_V2.1 α_1 II-III loop antibody (Alomone Labs, ACC-001,
273 rabbit polyclonal) diluted 1:500 (final concentration 1.7 µg/ml) were incubated overnight at 4°C to
274 blot the expression of Ca_V2.1/2.3 II-III loop hybrid construct, Ca_V2.3 α_1 CT antibody (Synaptic
275 Systems, #152 411, mouse monoclonal) diluted 1:500 (final concentration 2 µg/ml) was incubated
276 overnight at 4°C to blot the expression of Ca_V2.1/2.3 II-III loop CT and Ca_V2.1/2.3 CT chimeras,
277 Ca_V2.2 CT antibody (Synaptic Systems, #152 311, mouse monoclonal) diluted 1:1000 (final
278 concentration 2 µg/ml) was incubated overnight at 4°C to detect the expression of Ca_V2.1/2.2 CT
279 chimera. β-actin antibody (sigma, A2228, mouse monoclonal) diluted 1:5000 (final concentration
280 0.4 µg /ml) was incubated overnight at 4°C used to blot the expression of β-actin. Goat anti mouse
281 IgG (H+L) poly-HRP (Thermo Fisher, #32230) diluted 1:2000 (final concentration 0.25 µg /ml) and
282 goat anti rabbit IgG (H+L) poly-HRP (Thermo Fisher, #32260) secondary antibody diluted 1:2000
283 (final concentration 0.25 ng/ml) was incubated at room temperature for 1 hour. Protein bands

284 were detected by chemiluminescence using ECL Western blot detection reagents (Bio-Rad, #170-
285 5060).

286 **Preparation of acute slices**

287 Acute brain slices were prepared as previously described (Chen *et al.*, 2013). Briefly, after
288 decapitation of P9-11 mice of either sex, the brains were immersed in ice-cold low Ca^{2+} artificial
289 cerebrospinal fluid (aCSF) containing (in mM): 125 NaCl, 2.5 KCl, 3 $MgCl_2$, 0.1 $CaCl_2$, 10 glucose,
290 25 $NaHCO_3$, 1.25 Na_2HPO_4, 0.4 L-ascorbic acid, 3 myo-inositol, and 2 Na-pyruvate, pH 7.3-7.4
291 (310 mosmol/l). aCSF solution was continuously bubbled with 95% O_2 and 5% CO_2. Acute brain
292 slices (200 μm thickness) containing MNTB were obtained using a vibrating tissue slicer
293 (Campden 7000 smz-2, Campden Instruments LTD, Loughborough, England). Slices were
294 immediately transferred to standard aCSF (37°C, continuously bubbled with 95% O_2-5% CO_2)
295 containing the same chemicals as the slicing buffer except that it contained 1mM $MgCl_2$ and 1 mM
296 $CaCl_2$. After 1 hour incubation for recovery, slices were transferred to a recording chamber with
297 the same aCSF at room temperature (RT: 25°C).

298 **Acute slice electrophysiology**

299 In all experiments, slices were continuously perfused with aCSF and visualized by upright
300 microscope (BX51W, Olympus) through 4X air or 60X water-immersion objective (LUMPlanFL N,
301 Olympus, Tokyo, Japan) and a CCD camera (QI-Click, QImaging, Surrey, BC, Canada). Patch
302 clamp recordings were performed by using an EPC 10/2 patch-clamp amplifier (HEKA,
303 Lambrecht, Germany), operated by PatchMaster version 2x90.5 (Harvard Instruments, Holliston,
304 MA, USA). Data were low-pass filtered at 6 kHz and sampled with a rate of 50 kHz. Calyces
305 transduced with HdAd $Ca_V2.1$ α_1 chimeric constructs were identified visually with two co-
306 expressed mEGFP and mCherry markers. To visualize mEGFP and mCherry with light of 470 nm
307 or 560 nm, respectively, a Polychrome V xenon bulb monochromator or a lumen Metal arc lamp
308 was used (TILL Photonics, Grafelfing, Germany).

309 **Presynaptic Ca^{2+} current recordings**

310 To isolate presynaptic Ca^{2+} currents, aCSF was supplemented with 1 or 1.5 µM tetrodotoxin (TTX,
311 Alomone labs), 100 µM 4-aminopyridin (4-AP, Tocris) and 20 mM tetraethylammonium chloride
312 (TEA, Sigma Aldrich) to block Na^+ and K^+ channels. Calyces were whole-cell voltage clamped at
313 -80 mV. Current-voltage (IV) relationships were recorded in the presence of 1 mM $CaCl_2$ and 1
314 mM $MgCl_2$ with 1.5 µM TTX while pharmacological isolation of Ca_V2 subtype components was
315 performed in 2 mM $CaCl_2$ and 1 mM $MgCl_2$ with 1 µM TTX. To characterize the in the presynaptic
316 terminal, we used 200 nM ω-agatoxin IVA (Alomone labs) for selective inhibition of $Ca_V2.1$
317 channels, 2 µM ω-conotoxin GIVA (Alomone labs) for selective inhibition of $Ca_V2.2$ channels, 200
318 nM SNX-482 (Alomone labs) for selective inhibition of $Ca_V2.3$ channels, 10 µM Nifedipine
319 (Alomone labs) for selective inhibition of Ca_V1 chnannels and supplemented 0.1 mg/mL
320 cytochrome C to prevent toxin absorption. 50µM $CdCl_2$ was used for non-selective inhibition of
321 all VGCCs. Presynaptic patch pipette with open tip diameters 4-6 MΩ resistance were pulled from
322 1.5 mm thin-walled borosilicate glass (Harvard apparatus) and were filled with following internal
323 solution (in mM): 145 Cs-gluconate, 20 TEA-Cl, 10 HEPES, 2 Na_2-phosphocreatine, 4 MgATP,
324 0.3 NaGTP, and 0.075 EGTA, pH 7.2, 325-340 mOsm. Pipettes were coated with dental wax to
325 minimize stray capacitance and improve voltage clamp quality. Presynaptic series resistance was
326 less than 15 MΩ and was compensated online to 3 MΩ or less for IV recordings or compensated
327 to 6 MΩ for Ca_V2 subtype characterization experiments with a time lag of 10 µs by the HEKA
328 amplifier. Leak and capacitive currents were subtracted online with a P/5 routine. Cells with series
329 resistance >15 MΩ and leak currents > 100 pA were excluded from the analysis.

330 **Analysis of electrophysiological data**

331 All data was analyzed by NeuroMatic (Rothman & Silver, 2018) in Igor Pro (version 8.0,
332 Wavemetrics, Portland, OR, USA). Voltage dependence of channel activation was described by
333 both peak and tail currents as functions of voltage. Peak currents were fitted according to a
334 Hodgkin-Huxley formalism with four independent gates assuming a Goldman-Hodgkin-Katz
335 (GHK) open-channel conductance T: with E_{rev} as reversal potential, V_m as half-maximal activation

336 voltage per gate, and k_m as the voltage dependence of activation. Tail currents were measured
337 as peaks minus baseline and fitted with a Boltzmann function:

338 $$I(V) = \mathrm{T}\frac{1 - e^{-\frac{V-E_{rev}}{25mV}}}{1 - e^{-\frac{V}{25mV}}}\left(1 - e^{\frac{V-Vm}{Km}}\right)^{-4}$$

339

340 where $V_{1/2}$ represents the half-maximal voltage and k the corresponding slope factor.

341 **Statistical analysis**

342 All statistical tests were conducted in Prism 6 (GraphPad Software). Sample sizes for all
343 experiments were chosen based on assuming a population with a normal distribution sample size
344 of seven is sufficient to invoke the Central Limit Theorem. All data were tested for normal
345 distribution by performing a Shapiro-Wilk test for normality and variances of all data were
346 estimated and compared using Bartlett's test. Electrophysiological data were compared with one-
347 way analysis of variance (ANOVA) with a post hoc Dunnett's test, $Ca_V2.1$ FT dataset was used
348 as control group. In Figures and Table, data are reported as mean ± SD. Statistical significance
349 was accepted at *$p<0.05$; **$p<0.01$; ***$p<0.001$; ****$p<0.0001$.

350

351 **Results**

352 **$Ca_V2.1$ and $Ca_V2.2$ channels can be ablated at the calyx of Held in $Ca_V2.1/Ca_V2.2$ CKO**
353 **mouse model.**

354 Since ablation of $Ca_V2.1$ channels results in partial compensation of Ca_V2 current levels
355 by $Ca_V2.2$ channels at the calyx of Held (Inchauspe *et al.*, 2004; Lubbert *et al.*, 2017), we created
356 a $Ca_V2.1$/ $Ca_V2.2$ CKO mouse model (Fig. 1A) to allow for spatial and temporal ablation of $Ca_V2.1$
357 and $Ca_V2.2$ channels. To determine how presynaptic loss of $Ca_V2.1$ and $Ca_V2.2$ channels
358 impacted presynaptic Ca_V2 currents at the calyx of Held, we injected HdAd Cre at P1 into the
359 cochlear nucleus (CN) of $Ca_V2.1$/ $Ca_V2.2$ CKO mice to create a $Ca_V2.1^{-/-}$/ $Ca_V2.2^{-/-}$ calyx of Held.
360 Subsequently we performed whole-cell patch clamp recordings at the P9-11 calyx of Held and
361 characterized the total Ca^{2+} current and current sensitivity to Ca_V2 subtype-specific blockers: ω-
362 Agatoxin IVA (Aga), $Ca_V2.1$-specific, ω-Conotoxin GIVA (Cono), $Ca_V2.2$-specific, and Cadmium
363 (Cd^{2+}) a non-specific blocker of Ca_V currents (Fig. 1D-F, Table 1). Since sequential application of
364 blockers takes ~10-15 minutes for complete characterization of Ca_V2 currents, we measured
365 presynaptic Ca^{2+} current rundown at wild-type calyces in the absence of blockers after ~10-15
366 minutes (Fig. 1B, C). We found a ~20-70 pA (2-5%) reduction of presynaptic Ca^{2+} currents (Fig.
367 1J, Table 1, n=3). Subsequently, analysis of Ca^{2+} currents at the $Ca_V2.1^{-/-}$/ $Ca_V2.2^{-/-}$ calyx revealed
368 a significant reduction (wt vs. CKO (pA): -1078 ± 260.9 (n=10) vs. -425.5 ± 219.5 (n=11),
369 $p<0.0001$) (Fig. 1E, Table 2). We found an almost complete loss of Aga sensitive currents, 809
370 ± 255.6 (n=4) vs 99.22 ± 53.64 (n=5), p=0.0005; and Cono sensitive currents, 92 ± 142.2 (n=4)
371 vs 50.8 ± 43.1 (n=5), p=0.5532). (Fig1. D and F, Table 1). Therefore, these results demonstrate
372 successful ablation of $Ca_V2.1$ and $Ca_V2.2$ channels.

373 In the absence of $Ca_V2.1$ and $Ca_V2.2$, a significant Aga and Cono insensitive presynaptic
374 Ca^{2+} current was present. Since $Ca_V2.3$ subtypes can compensate for the loss of $Ca_V2.1$ channels
375 (Kaja *et al.*, 2006) and Ca_V1 channels can be found in some presynaptic terminals (Giugovaz-

376 Tropper *et al.*, 2011; Young & Veeraraghavan, 2021), it was important to determine if the
377 combined loss of $Ca_V2.1$ and $Ca_V2.2$ resulted in compensation by $Ca_V2.3$ or Ca_V1 channels.
378 Therefore, we characterized the sensitivity of presynaptic Ca^{2+} current to $Ca_V2.3$ and Ca_V1
379 specific blockers in the $Ca_V2.1^{-/-}$/ $Ca_V2.2^{-/-}$ calyx of Held. First, we used SNX-482, a $Ca_V2.3$
380 selective blocker and found a range of ~10% to 35% block of presynaptic Ca^{2+} currents (SNX-
381 482 sensitive fraction 24.33 ± 9.074 %) (n=3) (Fig. 1G, H, Table 1). Since there were variable
382 levels of Ca^{2+} current reduction with SNX-482, this indicated the remaining Ca^{2+} currents in the
383 absence of $Ca_V2.1$ and $Ca_V2.2$ could be mediated by a combination of $Ca_V2.3$ variants that are
384 SNX-482 sensitive and SNX-482 insensitive and/or presynaptic Ca_V1 channels. To determine if
385 Ca_V1 channels were present, we used nifedipine, a Ca_V1 selective blocker (Fig. 1I, J) and found
386 presynaptic Ca^{2+} currents were nifedipine insensitive as there was no difference compared to the
387 reduced fraction of Ca^{2+} current due to rundown (Fig. 1I, J, Table 1). Therefore, we conclude that
388 in the absence of $Ca_V2.1$ and $Ca_V2.2$ channels the compensatory presynaptic Ca^{2+} currents are
389 mediated by mix of SNX-482 sensitive and insensitive $Ca_V2.3$ channels.

390 **The $Ca_V2.1$ α_1 subunit loop II-III domain, and CT are positive regulators of presynaptic**
391 **$Ca_V2.1$ abundance**

392 The amino acid conservation of $Ca_V2.1$ α_1 subunit and $Ca_V2.3$ α_1 subunit loop II-III region
393 is 33.2% and CT region from aa. 1933 onwards is 39.8%, while the loop I-II is 87.3% conserved
394 (Figure 2A, MegAlign Pro 17, Clustal Omega). In fact, the $Ca_V2.3$ α_1 subunit loop II-III lacks a
395 syntaxin I binding site in the synprint region, while the $Ca_V2.3$ α_1 subunit CT lacks many of
396 proposed AZ protein binding motifs found in the $Ca_V2.1$ CT (Dolphin & Lee, 2020). Since the loop
397 II-III and CT regions are the most divergent, we created $Ca_V2.1$/$Ca_V2.3$ α_1 subunit chimeras that
398 swapped the loop II-III and CT domains to determine if these domains regulated presynaptic
399 $Ca_V2.1$ abundance and preference (Fig. 2B). We generated three HdAd $Ca_V2.1$/2.3 α_1 subunit
400 chimeric constructs (Figure 2C). There were <u>$Ca_V2.1$/2.3 II-III loop</u>, which contains the $Ca_V2.3$ α_1
401 subunit loop II-III domain (aa. 707 to aa. 1151), <u>$Ca_V2.1$/2.3 CT</u>, which contains the cytoplasmic

402 $Ca_V2.3$ CT (aa. 1897 to aa. 2273), and <u>$Ca_V2.1/2.3$ II-III+CT</u> which contains both the $Ca_V2.3$ α_1
403 subunit loop II-III and CT (Fig. 3C). To validate that the chimeras were expressed as full-length
404 proteins, we performed Western Blot analysis of HEK293 cells infected with our HdAd $Ca_V2.1/2.3$
405 chimeric constructs. Based on our results, we found that all constructs were successfully
406 expressed (Figure 2D-F).

407 Rescue experiments with an HdAd vector that expressed the $Ca_V2.1$ α_1 subunit FT (Mus
408 musculus NP_031604.3) (HdAd $Ca_V2.1$ FT) in the $Cav2.1^{-/-}$ calyx of Held in a *Cacna1a* CKO
409 mouse model has been validated to restore $Ca_V2.1$ current amplitudes, subtype levels and
410 synaptic vesicle release rates to similar levels as wild-type calyces (Lubbert *et al.*, 2017). To
411 validate our experimental approach, we used expressed the $Ca_V2.1$ α_1 subunit FT using HdAd
412 $Ca_V2.1$ FT on the $Ca_V2.1$,$Ca_V2.2$ CKO mouse line . Our rescue experiments show that HdAd
413 expression of the $Ca_V2.1$ FT in the $Ca_V2.1^{-/-}$/ $Ca_V2.2^{-/-}$ calyx of Held led to similar maximum Ca^{2+}
414 current amplitudes and voltage-dependent activation as the wild-type calyx of Held. These results
415 validated our experimental approach and confirming previous findings (Table 2).

416 Subsequently, we expressed the $Ca_V2.1/2.3$ chimeras and performed direct presynaptic
417 Ca^{2+} recordings. All chimera constructs were compared to $Ca_V2.1$ α_1 subunit FT and $Ca_V2.1^{-/-}$/
418 $Ca_V2.2^{-/-}$ calyces to determine rescue efficiency (Fig. 3). Since we did not find any differences in
419 the calyx of Held size with expression of the Ca_V2 chimeras (Table 8), we reported data as
420 maximal Ca^{2+} currents amplitude at all voltages. Current to voltage (IV) analysis revealed
421 significant reduction in peak Ca^{2+} current amplitudes with all three chimeras compared to $Ca_V2.1$
422 FT (Fig. 3, Table 3) However, only expression of the $Ca_V2.1/2.3$ loop II-III led to maximum Ca^{2+}
423 currents that were larger than that of the $Ca_V2.1^{-/-}$/ $Ca_V2.2^{-/-}$ (Maximum Ca^{2+} current amplitudes
424 (pA) $Ca_V2.1^{-/-}$/ $Cav2.2^{-/-}$: -425.5 ± 219.5 (n=11) vs. $Ca_V2.1/2.3$ II-III loop: -958.1 ± 331.3 (n=11),
425 $p<0.0001$) (Fig. 3E, Table 3). Based on these results, we demonstrate that $Ca_V2.1$ loop II-III and
426 $Ca_V2.1$ CT are positive regulators of presynaptic $Ca_V2.1$ abundance but differentially regulate
427 presynaptic $Ca_V2.1$ abundance.

428 **The $Ca_V2.1$ α_1 subunit loop II-III and $Ca_V2.1$ α_1 subunit CT do not independently control**
429 **$Ca_V2.1$ preference**

430 Ablation of Ca_V2 subtypes leads to increased presynaptic levels of other Ca_V2 subtypes
431 (Inchauspe *et al.*, 2004; Lubbert *et al.*, 2017) (Fig 1D, F), and overexpression of $Ca_V2.1$ results in
432 increased presynaptic $Ca_V2.1$ levels and competes away $Ca_V2.2$, but not vice versa (Lubbert *et*
433 *al.*, 2019). Therefore, it is postulated that presynaptic Ca_V2 abundance is correlated to Ca_V2
434 subtype preference. Although we found a reduction of presynaptic Ca^{2+} current with the
435 $Ca_V2.1/2.3$ chimeras, whether these regions regulated $Ca_V2.1$ preference or just abundance is
436 unknown. Therefore, it was important to elucidate if motifs that regulate presynaptic Ca_V2 subtype
437 abundance are also utilized to determine Ca_V2 subtype preference or if they were distinct. The
438 remaining Ca^{2+} currents from calyces expressing the $Ca_V2.1/2.3$ chimeras could be mediated by:
439 1) a mixture of $Ca_V2.1/2.3$ chimeras and $Ca_V2.3$ channels, 2) solely $Ca_V2.1/2.3$ chimeras, or 3)
440 solely $Ca_V2.3$ channels. Since the presynaptic Ca^{2+} currents in the $Ca_V2.1^{-/-}/Ca_V2.2^{-/-}$ calyx of
441 Held were completely Aga insensitive, and the $Ca_V2.1/2.3$ chimeras still maintain Aga binding
442 sites and are the Aga sensitive, we measured Aga sensitivity of Ca2+ currents with the $Ca_V2.1/2.3$
443 chimeras to distinguish between the different possibilities. In scenario 1, the $Ca_V2.1/2.3$ chimeras
444 are localized to the presynaptic membrane but do not completely away or only partially compete
445 away $Ca_V2.3$ channels and would result in a mix of Aga sensitive and insensitive Ca^{2+} currents.
446 In scenario 2, $Ca_V2.1/2.3$ chimeras are localized to the presynaptic membrane and compete away
447 $Ca_V2.3$ channels and would result in similar Aga sensitivity as the $Ca_V2.1$ FT. In scenario 3,
448 $Ca_V2.1/2.3$ chimeras are not localized to the presynaptic membrane with only $Ca_V2.3$ currents
449 remaining and would result in similar Aga insensitivity as the $Ca_V2.1^{-/-}$/ $Ca_V2.2^{-/-}$ calyx of Held.
450 Analysis of Aga sensitivity of $Ca_V2.1/2.3$ II-III or $Ca_V2.1/2.3$ CT showed no difference compared
451 to the $Ca_V2.1$ FT (Fig. 4, Table 4). However, we found partial Aga sensitivity with $Ca_V2.1/2.3$ II-
452 III+ CT (Aga sensitive fraction (%): $Ca_V2.1$ FT 89.5 ± 4.95 (n=3) vs. $Ca_V2.1/2.3$ II-III+ CT 67.67 ±
453 7.371 (n=3), p=0.0111) (Fig. 4, Table 4). Based on our data, we demonstrate that both $Ca_V2.1/2.3$

454 chimeras with the loop II-III or CT swap are able to compete away $Ca_V2.3$ channels (Fig. 4, Table
455 4). Therefore, we conclude that $Ca_V2.1$ loop II-III and the CT do not independently control $Ca_V2.1$
456 preference and motifs that regulate presynaptic $Ca_V2.1$ preference are distinct from those that
457 regulate presynaptic $Ca_V2.1$ abundance.

458 **The $Ca_V2.3$ α_1 subunit CT negatively regulates presynaptic $Ca_V2.1$ abundance while the**
459 **$Ca_V2.1$ CT aa. 1933-1966 positively regulates presynaptic $Ca_V2.1$ abundance**

460 The $Ca_V2.3$ CT contains a Calmodulin binding domain (CBD) but does not contain many
461 motifs postulated to mediate presynaptic $Ca_V2.1$ subtype abundance (Kamp *et al.*, 2012; Nanou
462 & Catterall, 2018). In addition, proposed $Ca_V2.1$ CT motifs (aa 2016 onwards) are not essential
463 determinants of presynaptic $Ca_V2.1$ abundance (Lubbert *et al.*, 2017). Thus, we hypothesized that
464 the 1) $Ca_V2.3$ CT acts as a negative regulator of presynaptic Ca_V2 abundance, and/or 2) the
465 $Ca_V2.1$ CBD regulates presynaptic Ca_V2 abundance. Therefore, to elucidate the mechanism of
466 action of the $Ca_V2.3$ CT, we created two additional $Ca_V2.1/2.3$ CT chimeras. They were the
467 <u>$Ca_V2.1/2.3$ CT 1967-2368</u>, which replaces the $Ca_V2.1$ CT with the $Ca_V2.3$ CT from $Ca_V2.1$ aa.
468 1967 onwards and contains the $Ca_V2.3$ CBD, and the <u>$Ca_V2.1/2.3$ CT 2016-2368</u> which replaces
469 the $Ca_V2.1$ CT with the $Ca_V2.3$ CT from $Ca_V2.1$ aa 2016 onwards (Fig. 5A). Subsequently, we
470 expressed these chimeras and $Ca_V2.1$ Δ2016, which deletes all motifs, AZ protein binding sites,
471 and the secondary $Ca_V\beta$ interaction site(Lubbert *et al.*, 2017) and measured their maximum Ca^{2+}
472 amplitudes to determine rescue efficiency (Fig. 5). As previously published. we found no
473 difference in maximum Ca^{2+} currents between $Ca_V2.1$ Δ2016 and $Ca_V2.1$ FT (Fig. 5B-C, Table 5),
474 thereby confirming that motifs in the $Ca_V2.1$ CT aa. 2016 onwards are not essential for controlling
475 presynaptic $Ca_V2.1$ abundance. In contrast, expression of $Ca_V2.1/2.3$ CT 2016-2368 and
476 $Ca_V2.1/2.3$ CT 1967-2368 resulted in a reduction in the maximum Ca^{2+} current amplitudes ($Ca_V2.1$
477 Δ2016: -1241 ± 207.4 (n=6) vs. $Ca_V2.1/2.3$ CT 2016-2368: -934.1 ± 210.6 (pA) (n=12), p=0.0209;
478 $Ca_V2.1$ Δ2016: -1241 ± 207.4 (n=6) vs. $Ca_V2.1/2.3$ CT 1967-2368: -839.5 ± 251.9 (pA) (n=8),
479 p=0.0047) (Fig. 5D-F, Table 5), but the maximum Ca^{2+} current amplitudes with either $Ca_V2.1/2.3$

480 CT 1967-2368 or $Ca_V2.1/2.3$ CT 2016-2368 were larger than the $Ca_V2.1/2.3$ CT 1933-2368 ((pA)
481 $Ca_V2.1/2.3$ CT aa. 1933-2368: -557.7 ± 198.9 (n=9) vs. $Ca_V2.1/2.3$ CT 2016-2368: -934.1 ± 210.6
482 (n=12), p=0.0013; $Ca_V2.1/2.3$ CT aa. 1933-2368: -557.7 ± 198.9 (n=9) vs. $Ca_V2.1/2.3$ CT 1967-
483 2368: -839.5 ± 251.9 (n=8), p=0.0321) (Fig. 5D-F, Table 5). Therefore, we conclude that the
484 $Ca_V2.3$ CT aa. 1952-2273 contains a motif or motifs that negatively regulate presynaptic $Ca_V2.3$
485 abundance and the $Ca_V2.1$ CBD is not a positive regulator of presynaptic $Ca_V2.1$ abundance.
486 Furthermore, we identified the region between $Ca_V2.1$ CT aa. 1933-1966 positively regulates
487 presynaptic $Ca_V2.1$ abundance.

488 **The $Ca_V2.2$ CT does not control presynaptic $Ca_V2.1$ abundance**

489 Since we identified that the $Ca_V2.3$ CT was a negative regulator of presynaptic $Ca_V2.3$
490 abundance, we set out to determine if this was unique to the $Ca_V2.3$ CT. Thus, to address if
491 $Ca_V2.2$ CT negatively regulated presynaptic Ca_V2 abundance, we created a $Ca_V2.1/2.2$ CT
492 chimera and cloned this into our HdAd vectors. Western blot analysis demonstrated no issues
493 with expression of the $Ca_V2.1/2.2$ CT chimera (Fig. 6A). Subsequently we expressed the
494 $Ca_V2.1/2.2$ CT chimera and performed IV analysis on presynaptic Ca^{2+} currents. Results of our
495 IV analysis revealed that there was no difference in the maximum Ca^{2+} current between the
496 $Ca_V2.1/2.2$ CT chimera and $Ca_V2.1$ FT (Fig. 6B-E). However, compared to $Ca_V2.1$ FT, there
497 appeared to be unequal variances of maximum Ca^{2+} current amplitudes with $Ca_V2.1/2.2$ CT that
498 was marginally significant (F-test comparing variances p=0.0607) (Fig. 6B-E, Table 6). Therefore,
499 our data suggests that the $Ca_V2.2$ CT is not a negative regulator of presynaptic abundance

500 **High level overexpression of $Ca_V2.1/2.2$ CT rescues presynaptic Ca^{2+} currents while**
501 **$Ca_V2.1/2.3$ CT does not.**

502 High level overexpression of $Ca_V2.1$ α_1 subunit results in increased presynaptic $Ca_V2.1$
503 levels and compete away $Ca_V2.2$ and $Ca_V2.3$ channels, however high-level overexpression of
504 $Ca_V2.2$ α_1 subunit does not result in a reduction of $Ca_V2.1$ levels at the calyx of Held (Lubbert *et*
505 *al.*, 2019). This suggests that upstream regulatory steps, such as protein trafficking and

506 membrane insertion steps, are integral to $Ca_V2.1$ level preference and abundance (Ferron *et al.*,
507 2021; Young & Veeraraghavan, 2021). It is known that high levels of overexpression can saturate
508 regulatory steps that control trafficking (Lubbert *et al.*, 2019). Therefore, to determine if these
509 regulatory step(s) could be saturated, we used the high-level overexpression Pun cassette
510 (Young & Neher, 2009; Montesinos *et al.*, 2011; Lubbert *et al.*, 2019) to drive expression of
511 $Ca_V2.1/2.2$ CT and $Ca_V2.1/2.3$ CT chimeras and determine if we could increase the presynaptic
512 Ca_V2 chimera current levels and compared their maximum Ca^{2+} current amplitudes to Pun $Ca_V2.1$
513 FT. We found no difference in presynaptic Ca^{2+} currents with Pun $Ca_V2.1/2.2$ CT compared to
514 Pun $Ca_V2.1$ FT (Fig. 7, Table 7). However, maximum Ca^{2+} current amplitudes with Pun $Ca_V2.1/2.3$
515 CT were lower than Pun $Ca_V2.1$ FT (Pun $Ca_V2.1$ FT: -1438 ± 263.9 (n=7) vs. Pun $Ca_V2.1/2.3$ CT:
516 -772.8 ± 291.8 (n=10), (pA), p=0.0006) (Fig. 7, Table 7). Moreover, the maximum Ca^{2+} current
517 amplitudes with Pun $Ca_V2.1/2.3$ CT showed no significant difference than syn $Ca_V2.1/2.3$ CT (Fig.
518 7, Table 7). Therefore, we demonstrate that the $Ca_V2.2$ CT is not a negative regulator of
519 presynaptic $Ca_V2.2$ abundance and the $Ca_V2.1/2.2$ CT chimera can be forced to increase
520 expression level, however, the negative regulator motif in $Ca_V2.3$ CT restrains the upstream
521 regulatory steps which results in low abundance of $Ca_V2.3$ channels in the presynaptic terminal.
522

523 **Discussion**

524 In this study, we provide insight into how presynaptic Ca_V2 subtype abundance is
525 determined by the Ca_V2 α_1 subunit. Based on our data, we demonstrate that the cytoplasmic loop
526 II-III and CT regions of the $Ca_V2.1$ α_1 subunit are positive regulators of presynaptic Ca_V2
527 abundance, while $Ca_V2.3$ CT negatively regulates presynaptic Ca_V2 abundance. In addition, we
528 find that $Ca_V2.2$ CT is not a key determinant of presynaptic Ca_V2 abundance. Furthermore, we
529 demonstrate that $Ca_V2.1$ α_1 subunit cytoplasmic loop II-III and CT regions do not independently
530 control presynaptic $Ca_V2.1$ preference. Therefore, we propose that the motifs controlling
531 presynaptic $Ca_V2.1$ preference are distinct from those regulating $Ca_V2.1$ levels and they may act
532 synergistically in pathways that regulate presynaptic $Ca_V2.1$ preference and levels.

533 **The Ca_V2 α_1 subunit II-III loop regulation of presynaptic $Ca_V2.1$ abundance.**

534 By swapping the loop II-III domain between $Ca_V2.1$ and $Ca_V2.3$ we demonstrated that the
535 $Ca_V2.1$ loop II-III region positively regulates presynaptic $Ca_V2.1$ abundance but does not regulate
536 preference. All Ca_V2 subunit loop II-III domains contain a synprint region which is the site of
537 interaction between the SNARE proteins syntaxin and SNAP-25 (Zhong *et al.*, 1999; Mochida *et*
538 *al.*, 2003; Yokoyama *et al.*, 2005). Although $Ca_V2.3$ currents are modulated by syntaxin (Wiser *et*
539 *al.*, 2002; Kamp *et al.*, 2005), the proposed syntaxin binding domain found in $Ca_V2.1$ and $Ca_V2.2$
540 is not found in the $Ca_V2.3$ α_1 subunit synprint region (Kamp *et al.*, 2005; Yokoyama *et al.*, 2005;
541 Rajapaksha *et al.*, 2008). Our findings that $Ca_V2.1/2.3$ loop II-III chimera resulted in presynaptic
542 Ca^{2+} current reduction indicates that potential differences in syntaxin binding between the different
543 subtypes of Ca_V2 α_1 subunits regulates presynaptic Ca_V2 abundance. Studies from cultured
544 hippocampal neurons, $Ca_V2.1$ dominant presynaptic terminals, found that partial deletions in the
545 $Ca_V2.2$ synprint region that impact SNARE binding resulted in less efficient $Ca_V2.2$ targeting to
546 presynaptic terminal (Szabo *et al.*, 2006). Similar partial deletions in the $Ca_V2.1$ synprint region
547 reduced $Ca_V2.1$ localization to release sites in cultured superior cervical ganglion (SCG) neurons
548 which utlize $Ca_V2.2$ dominant presynaptic terminals (Mochida *et al.*, 2003). In addition, splice

549 variants of $Ca_V2.1$ lacking the synprint region reduce incorporation into neuroendocrine cells
550 (Rajapaksha *et al.*, 2008). Since partial deletions of $Ca_V2.2$ synprint do not impair axonal
551 targeting(Szabo *et al.*, 2006), it is possible that the $Ca_V2.3$ synprint region does not regulate
552 axonal trafficking but rather regulates incorporation into the presynaptic terminal. Although the
553 $Ca_V2.3$ synprint region chimera resulted in reduced presynaptic Ca_V2 chimera levels, there was
554 no change in the proportion of Agatoxin sensitive currents. Therefore, this indicates the
555 mechanisms that control $Ca_V2.1$ preference are not determined by the loop II-III region binding
556 interactions.

557 **The Ca_V2 α_1 subunit CT differentially regulates presynaptic Ca_V2 subtype abundance.**

558 We found that the $Ca_V2.2$ CT and $Ca_V2.3$ CT had differential effects on presynaptic Ca_V2
559 abundance but did not impact Ca_V2 preference. Our data demonstrated that $Ca_V2.1/2.3$ CT
560 chimera results in a severe reduction in presynaptic Ca^{2+} currents and suggested that the $Ca_V2.3$
561 CT is a negative regulator of presynaptic $Ca_V2.3$ abundance. Prior studies (Lubbert *et al.*, 2017)
562 and our findings here revealed that the $Ca_V2.1$ CT Δ2016, which deletes multiple AZ protein
563 binding sites and other motifs restores presynaptic Ca^{2+} to $Ca_V2.1$ FT levels. These data
564 demonstrate these interactions and motifs are not essential for controlling presynaptic $Ca_V2.1$
565 abundance. However, replacing the $Ca_V2.1$ CT from aa. 2016 onwards with corresponding $Ca_V2.3$
566 CT aa. 1952-2273 resulted in a reduction of presynaptic Ca^{2+} currents compared to $Ca_V2.1$ CT
567 Δ2016. Furthermore, overexpression of $Ca_V2.1/2.3$ CT chimera by pUNISHER cassette was
568 similar to presynaptic Ca^{2+} currents levels with the low-level synapsin expression cassette. Based
569 on our data that showed the $Ca_V2.1$ CT aa. 2016-2368 is dispensable for $Ca_V2.1$ abundance, we
570 propose that $Ca_V2.3$ CT aa. 1952-2273 contains a motif that prevents presynaptic Ca_V2 targeting
571 or incorporation into the plasma membrane. In addition, our results indicate that CT dependent
572 mechanism of regulation of presynaptic Ca_V2 abundance is dominant to the loop II-III region
573 mechanisms of action as $Ca_V2.1/2.3$ CT chimera resulted in significantly lower presynaptic Ca^{2+}

574 currents than those with the $Ca_V2.1/2.3$ loop II-III.

575 Calmodulin (CaM) is considered a core component of Ca_V2 channel complexes and
576 interacts with the Cav2.1 channels through a bipartite interaction with the calmodulin binding
577 domain (CBD) and IQ-like motif (IM) domain to regulate calcium dependent facilitation (CDF) and
578 inactivation (CDI) (Lee *et al.*, 2003; Chaudhuri *et al.*, 2004; Mori *et al.*, 2008). However, how CaM
579 interactions regulate presynaptic $Ca_V2.1$ levels is unclear. The $Ca_V2.1/2.3$ CT aa. 1967-2368
580 chimera, which replaces the $Ca_V2.1$ CBD with the $Ca_V2.3$ CBD, showed no difference in rescuing
581 efficiency compared to $Ca_V2.1/2.3$ CT aa. 2016-2368 chimeras. However, we found that
582 presynaptic Ca^{2+} currents with $Ca_V2.1/2.3$ CT aa. 1967-2368 chimera were larger than that with
583 $Ca_V2.1/2.3$ CT aa. 1933-2368 chimera. Therefore, our results demonstrated that the $Ca_V2.1$ CBD
584 does not control presynaptic $Ca_V2.1$ abundance but the linker region of $Ca_V2.1$ CT aa. 1933-1966
585 between the IQ domain and the CBD plays a role in regulation of $Ca_V2.1$ levels. Since the
586 CaM/CBD complex interacts with the IM domain (Nanou *et al.*, 2016; Serra *et al.*, 2018), it is
587 possible that the $Ca_V2.3$ CBD and linker region with $Ca_V2.1$ IQ domain result in a different
588 structural conformation of the CT that impacts presynaptic Ca_V2 abundance. Interestingly, the
589 combination of the mutation (IM-AA) in the IM domain and CBD deletion in SCG neurons results
590 in an increased peak Ca^{2+} currents levels, while the IM-AA or CBD deletion alone did not alter
591 Ca^{2+} current levels (Mochida *et al.*, 2008). Therefore, the IQ domain and CBD may synergistically
592 regulate $Ca_V2.1$ level. However, the molecular mechanisms how these regions impact $Ca_V2.1$
593 abundance is unknown and future experiments are needed.

594 In contrast to the $Ca_V2.1/2.3$ CT chimera, we found no difference in the average
595 presynaptic Ca^{2+} current levels with the $Ca_V2.1/2.2$ CT chimera compared to $Ca_V2.1$ FT. However,
596 we observed a large variability of Ca^{2+} current amplitudes with $Ca_V2.1/2.2$ CT that is marginally
597 significant compared to $Ca_V2.1$ FT rescue. Therefore, our data implies that the $Ca_V2.2$ CT is not
598 a key determinant of presynaptic Ca_V2 abundance. Unlike the $Ca_V2.3$ CT, high level
599 overexpression of $Ca_V2.1/2.2$ CT resulted in similar presynaptic Ca^{2+} current levels compared to

600 high level overexpression of $Ca_V2.1$ FT level and no change in variability. Therefore, we propose
601 that the $Ca_V2.2$ CT does not contain motifs that prevents presynaptic $Ca_V2.2$ targeting or
602 incorporation into the plasma membrane.

603 **Ca_V2 subtype abundance and preference are regulated by distinct pathways.**

604 Although there were differences in the presynaptic Ca^{2+} current levels with the $Ca_V2.1/2.3$
605 loop II-III and $Ca_V2.1/2.3$ CT chimeras, they had similar Aga sensitivity as presynaptic Ca^{2+}
606 currents with the $Ca_V2.1$ FT. However, there was a significant Aga insensitive component of Ca^{2+}
607 currents with $Ca_V2.1/2.3$ loop II-III+ CT chimera despite having similar Ca^{2+} current levels as the
608 $Ca_V2.1/2.3$ CT and $Ca_V2.1^{-/-}$/ $Ca_V2.2^{-/-}$ background. Therefore, our data indicates that: 1)
609 Presynaptic Ca_V2 subtype abundance mechanisms are independent of those that control
610 preference. 2) The loop II-III region and the CT region do not individually encode preference. 3)
611 The $Ca_V2.1$ II-III loop and CT region may act synergistically to control Ca_V2 subtype preference.
612 4) Other motifs in the $Ca_V2.1$ α_1 subunit outside of the CT and synprint region are involved in
613 regulating presynaptic Ca_V2 subtype preference. Potential candidates that may control preference
614 are the Ca_V2 α_1 subunit at AID in domain I-II which binds to the $Ca_V\beta$ subunit with high affinity(De
615 Waard *et al.*, 1994). $Ca_V\beta$ subunits are critical for regulating Ca_V2 trafficking and $Ca_V\beta4$ and
616 $Ca_V\beta2a$ are located within the presynaptic terminal. $Ca_V2.1$ channels have higher specificity for
617 binding to $Ca_V\beta4$ than $Ca_V2.2$ and $Ca_V2.3$ channels (Xie *et al.*, 2007; Muller *et al.*, 2010). Another
618 possibility is that preference is not encoded by motifs in the cytoplasmic regions but is controlled
619 by the Cacna2d protein family (Dolphin, 2012; Hoppa *et al.*, 2012; Stephani *et al.*, 2019). Knockout
620 of $\alpha_2\delta3$ subunit in spiral ganglion neurons results in reduced $Ca_V2.1$ and $Ca_V2.3$ components with
621 no change in $Ca_V2.2$ subtype levels (Stephani *et al.*, 2019). In contrast overexpression of $\alpha_2\delta1$
622 subunit decreases $Ca_V2.2$ level in cultured hippocampal neurons (Pilch *et al.*, 2022), but did not
623 change other Ca_V2 subtype levels. Furthermore, the globular bushy cells which give rise to the
624 calyx of Held, only express *Cacna2d2* and *Cacna2d3*. In addition, other synapses that undergo
625 developmental reduction of $Ca_V2.2$ and $Ca_V2.3$ express *Cacna2d1*. Finally, the $\alpha_2\delta$ binding

626 preference does not correlate to presynaptic Ca_V2 subtype levels (Voigt *et al.*, 2016) while
627 CACNA2D expression patterns do not correlate to presynaptic Cav2 subytpe levels (Cole *et al.*,
628 2005). Therefore, given these conflicting findings more experiments will be needed to decipher if
629 the Cacna2d proteins regulate preference.

630 While it is possible that the loop II-III domain and the CT domain act in concert to regulate
631 presynaptic preference, it is also possible that they are not involved in preference mechanisms
632 but rather combination of the loop II-III and CT domain swap construct dramatically impair the
633 Ca_V2 chimera trafficking to the presynaptic terminal. In this scenario, the $Ca_V2.1/2.3$ II-III loop+
634 CT chimera does not effectively compete away native $Ca_V2.3$ channels, which are normally
635 restricted from the upstream pathways that regulate presynaptic trafficking. Therefore, native
636 $Ca_V2.3$ channels are also trafficked to the presynaptic terminals that express the $Ca_V2.1/2.3$ II-III
637 loop+ CT chimera. In this hypothetical scenario, the preference mechanism(s) has high affinity for
638 the $Ca_V2.1/2.3$ chimera channel and low affinity for the $Ca_V2.3$ channels, however by law of mass
639 action, $Ca_V2.3$ channels now participate in molecular pathways that determine preference and
640 results in the presence of presynaptic $Ca_V2.3$ channels. Based on our model, this demonstrates
641 how alternative splicing of the Ca_V2 α_1 subunits and potentially alternative splicing of molecules
642 in pathways that control Ca_V2 trafficking (Weiss & Zamponi, 2017), and insertion into the
643 membrane may lead to developmentally changes in presynaptic Ca_V2 subtype levels. However,
644 the molecular machinery and the motifs that determine preference remain to be identified.

645 By demonstrating that motifs in the Ca_V2 α_1 subunit that control presynaptic Ca_V2 subtype
646 abundance are distinct from those determining presynaptic Ca_V2 subtype preference, our findings
647 provide new insights into the regulation of presynaptic Ca_V2 subtype levels.

648

649

650

651

652

653 **Figure legends**

654 **Figure 1. Presynaptic $Ca_V2.1$ and $Ca_V2.2$ channels can be ablated and the remaining Ca^{2+}**

655 **currents are compensated by $Ca_V2.3$ channels at the calyx of Held.**

656 (A) Illustration of CKO mouse model. Exon 4 of *Cacna1a*, and exons 5 and 6 of *Cacna1b* are

657 flanked by LoxP sites. (B-C) Example traces of Ca^{2+} currents and bar graph show rundown

658 fraction of electrophysiological recordings at duration of 10~15min at wildtype calyx of Held (n=3).

659 (D) Pharmacological isolation of presynaptic Ca_V2 isoforms in wildtype and $Ca_V2.1^{-/-}$/ $Ca_V2.2^{-/-}$

660 calyces. Ca^{2+} current traces in absence of any blockers (black), after blocking $Ca_V2.1$ fraction with

661 200 nM Aga (orange), after blocking $Ca_V2.2$ fraction with 2 mM Cono (blue) and after blocking all

662 Ca_V channels with 50 mM Cd^{2+} (gray). (E) Bar graph shows total Ca^{2+} currents in wildtype and

663 $Ca_V2.1^{-/-}$/ $Ca_V2.2^{-/-}$ calyces. (F) Relative Ca_V2 subtype fractions in wildtype, $Ca_V2.1^{-/-}$/ $Ca_V2.2^{-/-}$

664 calyces (n=3-5 for each condition). (G) Ca^{2+} current traces in absence of any blockers (black),

665 after blocking $Ca_V2.3$ fraction with 200 nM SNX-482 (green). (H) Bar graph shows SNX-482

666 sensitive fraction at $Ca_V2.1^{-/-}$/ $Ca_V2.2^{-/-}$ calyces (n=3). (I) Ca^{2+} current traces in absence of any

667 blockers (black), after blocking Ca_V1 fraction with 10 μM Nifedipine (red). (J) Bar graph shows the

668 reduction fraction and Ca^{2+} current amplitudes in $Ca_V2.1^{-/-}$/ $Ca_V2.2^{-/-}$ calyces after Nifedipine

669 treatment compared to wildtype rundown fraction.

670 **Figure 2. $Ca_V2.1/Ca_V2.3$ Chimeras can be efficiently expressed**

671 Western Blot validated protein expression of Ca_V2 hybrid constructs. HEK293 cells are infected

672 by HdAd $Ca_V2.1/2.3$ chimeric constructs. (A) Illustration of Ca_V2 α_1 structure. Four transmembrane

673 domains are highly conserved while the cytoplasmic loops are highly variant between $Ca_V2.1$ and

674 $Ca_V2.3$, the I-II loop, II-III loop and CT share 87.3%, 33.2% and 39.8% consensus, respectively.

675 (B) Illustration of swapped region between $Ca_V2.1$ and $Ca_V2.3$ channels, the amino acid numbers

676 are labelled. (C) Illustration of three $Ca_V2.1/2.3$ chimeric constructs. $Ca_V2.1$ II-III loop and CT are

677 both replaced by $Ca_V2.3$ II-III loop and CT in $Ca_V2.1/2.3$ II-III loop + CT chimeric construct. $Ca_V2.1$

678 II-III loop is replaced by $Ca_V2.3$ II-III loop in $Ca_V2.1/2.3$ II-III loop chimeric construct. $Ca_V2.1$ CT is
679 replaced by $Ca_V2.3$ CT in $Ca_V2.1/2.3$ CT chimeric construct. (D) Antibody targeting $Ca_V2.1$ CT
680 shows the protein expression of $Ca_V2.1$ FT and $Ca_V2.1/2.3$ II-III loop. (E) Antibody targeting
681 $Ca_V2.1$ II-III loop fails to detect protein expression of $Ca_V2.1/2.3$ II-III loop and $Ca_V2.1/2.3$ II-III
682 loop CT, indicating that the II-III loop of $Ca_V2.1$ is swapped by $Ca_V2.3$ II-III loop. (F) Antibody
683 targeting $Ca_V2.3$ CT shows the protein expression of $Ca_V2.1/2.3$ II-III loop CT and $Ca_V2.1/2.3$ CT.
684 Mock, negative control, protein lysis from uninfected HEK293 cells.

685 **Figure 3. The $Ca_V2.1/2.3$ α_1 CT chimera cannot rescue Ca^{2+} currents to $Ca_V2.1$ FT levels,**
686 **however the $Ca_V2.1/2.3$ loop II-III chimera partially rescues Ca^{2+} currents.**

687 (A) Sample traces of Ca^{2+} current triggered by 50 ms voltage steps from -60 mV to -30 mV in 10
688 mV steps, -25 mV to +20 mV in 5 mV steps, and +30 mV to +60 mV in 10 mV steps. Black: calyces
689 expressing $Ca_V2.1$ FT. Yellow: $Ca_V2.1^{-/-}$/ $Ca_V2.2^{-/-}$ calyces. Red: calyces expressing $Ca_V2.1/2.3$ II-
690 III loop CT chimeric construct. Blue: calyces expressing $Ca_V2.1/2.3$ II-III loop chimeric construct.
691 Gray: calyces expressing $Ca_V2.1/2.3$ CT chimeric construct. (B-C) IV relationship of Ca^{2+} currents
692 (B) and normalized Ca^{2+} currents by maximal Ca^{2+} currents (I/I_{max}; C) plotted against voltage
693 steps. (D-E) Bar graph shows absolute peak Ca^{2+} current amplitudes, one-way ANOVA, Dunnett's
694 test, $Ca_V2.1$ FT is used as positive control (D) and $Ca_V2.1^{-/-}$/ $Ca_V2.2^{-/-}$ is used as negative control
695 (E).

696 **Figure 4. The $Ca_V2.1/2.3$ $\alpha_1$subunit chimeras compete away $Ca_V2.3$ channel in the calyx of**
697 **Held.**

698 (A) Agatoxin isolation of presynaptic $Ca_V2.1/2.3$ chimeras in calyces expressing $Ca_V2.1$ FT (black,
699 n=3), $Ca_V2.1/2.3$ II-III loop CT (red, n=3), $Ca_V2.1/2.3$ II-III loop (blue, n=4), and $Ca_V2.1/2.3$ CT
700 (gray, n=3). Basal and reduced Ca^{2+} current traces after applying 200 nM ω-Aga IVA are labelled.
701 (B) Reduction of Agatoxin sensitive Ca^{2+} current over time. Ca^{2+} current amplitudes are plotted
702 against time, 200 nM ω-Aga IVA was applied at 5th pulse (50s). (C) Bar graph shows the ω-Aga

703 IVA sensitive reduction fraction in calyces expressing $Ca_V2.1$ FT, $Ca_V2.1/2.3$ II-III loop CT,
704 $Ca_V2.1/2.3$ II-III loop, and $Ca_V2.1/2.3$ CT.

705 **Figure 5. The $Ca_V2.3$ CT negatively regulates presynaptic Ca_V2 abundance, while the**
706 **$Ca_V2.1$ CT region aa. 1933-1966 promotes $Ca_V2.1$ abundance**

707 (A) Amino acid alignment of $Ca_V2.1$ and $Ca_V2.3$ CT. Sequences on top and bottom represent
708 $Ca_V2.1$ CT and $Ca_V2.3$ CT, respectively. Amino acid numbers of swapped sites in three $Ca_V2.1/2.3$
709 chimeras are indicated in black. $Ca_V2.1$ CBD is highlighted in green. (B) Example Ca^{2+} current
710 traces to 50 ms depolarization from -80mV holding potential to the maximal activation voltage
711 step (-15mV to +15mV, 5 mV steps) for $Ca_V2.1$ FT (black, n=11) and $Ca_V2.1$ Δ2016 (red, n=6).
712 (C) Bar graph shows absolute peak Ca^{2+} currents amplitude between $Ca_V2.1$ CT and $Ca_V2.1$
713 Δ2016, unpaired t test. (D) Example Ca^{2+} current traces to 50ms depolarization from -80mV
714 holding potential to the maximal activation voltage step (-15mV to +15mV, 5 mV steps) for $Ca_V2.1$
715 Δ2016, $Ca_V2.1/2.3$ CT aa. 2016-2368 (n=12); $Ca_V2.1/2.3$ CT 1967-2368 (n=8) and $Ca_V2.1/2.3$ CT
716 1933-2368 (n=9). (E-F) Bar graph shows peak Ca^{2+} currents amplitude, one-way ANOVA,
717 Dunnett's test, $Ca_V2.1$ Δ2016 is used as positive control (E) and $Ca_V2.1/2.3$ CT aa. 1933-2368 is
718 used as negative control (F).

719 **Figure 6. $Ca_V2.1/2.2$ CT chimera can be efficiently expressed and rescues Ca^{2+} currents to**
720 **$Ca_V2.1$ FT level with high variability.**

721 (A) Western Blot validated protein expression of $Ca_V2.1/2.2$ CT. HEK293 cells are infected by
722 HdAd $Ca_V2.1/2.2$ CT and $Ca_V2.2$ FT. Antibody targeting $Ca_V2.2$ CT shows the protein expression
723 of $Ca_V2.2$ FT and $Ca_V2.1/2.2$ CT. Mock, negative control, protein lysis from uninfected HEK293
724 cells. (B) Exemplary Ca^{2+} currents triggered by 50 ms voltage steps from -60 mV to -30 mV in 10
725 mV steps, -25 mV to +20 mV in 5 mV steps, and +30 mV to +60 mV in 10 mV steps. Black: calyces
726 expressing $Ca_V2.1$ FT (n=11). Yellow: $Ca_V2.1^{-/-}$/ $Ca_V2.2^{-/-}$ calyces (n=11). Green: calyces
727 expressing $Ca_V2.1/2.2$ CT (n=11), two phenotypes are demonstrated. (C-D) IV relationship of

728 Ca^{2+} currents (C) and normalized Ca^{2+} currents by maximal Ca^{2+} currents (I/I_{max}; D) plotted against
729 voltage steps. (E) Bar graph shows absolute peak Ca^{2+} current amplitudes. One-way ANOVA,
730 Dunnett's test, $Ca_V2.1$ FT is used as positive control, $Ca_V2.1^{-/-}$/ $Ca_V2.2^{-/-}$ is used as negative
731 control.

732 **Figure 7. High level overexpression of the $Ca_V2.1/2.3$ α_1 CT cannot rescue Ca^{2+} currents to**
733 **Pun $Ca_V2.1$ levels while Pun $Ca_V2.1/2.2$ α_1 CT can.**

734 (A) High-level overexpression cassette pUNISHER (Pun) is used to drive $Ca_V2.1$ FT, $Ca_V2.1/2.2$
735 CT and $Ca_V2.1/2.3$ CT chimeric constructs. Example Ca^{2+} current traces to 50ms depolarization
736 from -80mV holding potential to the maximal activation voltage step (-15mV to +15mV, 5 mV
737 steps) for calyces expressing Pun $Ca_V2.1$ FT (green, n=7), Pun $Ca_V2.1/2.2$ CT (purple, n=9) and
738 Pun $Ca_V2.1/2.3$ CT (orange, n=10) (B) Bar graph shows averaged peak Ca^{2+} currents for Pun
739 $Ca_V2.1$ FT, Pun $Ca_V2.1/2.2$ CT and Pun $Ca_V2.1/2.3$ CT constructs. One-way ANOVA, Dunnett's
740 test, Pun $Ca_V2.1$ FT is used as positive control.

741

742

743

744

745

746

747

748

749

750

751

752 **Table1. *Cacna1a, Cacna1b* $^{flox/flox}$ animal characterization.**

753

Parameter	Mean	SD	n	P	statistics
Wildtype animal					
Agatoxin sensitive fraction (%)	79.09	14.98	4		
Agatoxin sensitive currents (pA)	809.3	255.6	4	control	
Conotoxin sensitive fraction (%)	7.828	10.5	4		
Conotoxin sensitive currents (pA)	92.00	142.2	4		
$Ca_V2.1^{-/-}$/ $Ca_V2.2^{-/-}$					
Agatoxin sensitive fraction (%)	13.64	6.24	5	p<0.0001 (****)	
Agatoxin sensitive currents (pA)	99.22	53.64	5	p=0.0005 (***)	
Conotoxin sensitive fraction (%)	11.92	4.722	5	p=0.4571 (n.s.)	Unpaired t test
Conotoxin sensitive currents (pA)	50.80	43.10	5	p=0.5532 (n.s.)	
SNX-482 sensitive fraction (%)	24.33	9.074	3		
SNX-482 sensitive currents (pA)	86.65	31.26	3		
Rundown fraction					
Wildtype animal (pA)	43.70	20.85	3	control	Unpaired t test
$Ca_V2.1^{-/-}$/ $Ca_V2.2^{-/-}$ (pA)	51.40	23.78	3		
Wildtype animal (%)	3.167	0.6525	3	control	Unpaired t test
$Ca_V2.1^{-/-}$/ $Ca_V2.2^{-/-}$ (%)	8.393	4.169	3	P=0.0985	

754

755

756 **Table2. Electrophysiological parameters of IV relations of Ca^{2+} currents.**

757

Parameter	Mean	SD	n	P	statistics
Max. Ca^{2+} current amplitude I_{max} (pA)					
Wildtype (positive control)	-1078	260.9	10	control	One-Way ANOVA
$Ca_V2.1$ FT	-1222	256.2	11	p=0.3140 (n.s.)	Dunnett's Test
$Ca_V2.1^{-/-}$/ $Cav2.2^{-/-}$	-425.5	219.5	11	p<0.0001 (****)	
Wildtype	-1078	260.9	10	p<0.0001 (****)	One-Way ANOVA
$Ca_V2.1$ FT	-1222	256.2	11	p<0.0001 (****)	Dunnett's Test
$Ca_V2.1^{-/-}$/ $Cav2.2^{-/-}$ (negative control)	-425.5	219.5	11	control	
IV fit: Half-maximal activation voltage V_m (mV)					

Wildtype (control)	-21.61	5.205	10	positive control	One-Way ANOVA
$Ca_V2.1$ FT	-19.75	3.212	11	p=0.5848 (n.s.)	Dunnett's test
$Ca_V2.1^{-/-}$/ $Cav2.2^{-/-}$	-12.38	5.791	11	p=0.0003 (***)	
IV fit: Voltage-dependence of activation K_m (mV)					
Wildtype (control)	2.948	1.673	10	positive control	One-Way ANOVA
$Ca_V2.1$ FT	2.854	0.7658	11	p=0.9918 (n.s.)	Dunnett's test
$Ca_V2.1^{-/-}$/ $Cav2.2^{-/-}$	8.123	3.005	11	p<0.0001 (****)	
Boltzmann fit: Half-maximal activation voltage $V_{0.5}$ (mV)					
Wildtype (control)	-19.6	5.029	10	positive control	One-Way ANOVA
$Ca_V2.1$ FT	-17.29	4.761	11	p=0.4829 (n.s.)	Dunnett's test
$Ca_V2.1^{-/-}$/ $Cav2.2^{-/-}$	-14.82	5.428	11	p=0.0716 (n.s.)	
Boltzmann fit: Voltage-dependence K (mV)					
Wildtype (control)	3.654	1.981	10	positive control	One-Way ANOVA
$Ca_V2.1$ FT	5.052	5.07	11	p=0.5672 (n.s.)	Dunnett's test
$Ca_V2.1^{-/-}$/ $Cav2.2^{-/-}$	5.756	2.624	11	p=0.3036 (n.s.)	

758
759 **Table3. Electrophysiological parameters of IV relations of Ca^{2+} currents.**
760

Parameter	Mean	SD	n	P	statistics
Max. Ca^{2+} current amplitude I_{max} (pA)					
$Ca_V2.1$ FT (positive control)	-1222	256.2	11	control	
$Ca_V2.1^{-/-}$/ $Cav2.2^{-/-}$	-425.5	219.5	11	p<0.0001 (****)	One-Way ANOVA
Cav2.1/2.3 II-III loop CT	-470.5	112.6	8	p<0.0001 (****)	Dunnett's Test
Cav2.1/2.3 II-III loop	-958.1	331.3	11	p=0.0479 (*)	
Cav2.1/2.3 CT	-557.7	198.9	9	p<0.0001 (****)	
$Ca_V2.1$ FT	-1222	256.2	11	p<0.0001 (****)	
$Ca_V2.1^{-/-}$/ $Cav2.2^{-/-}$ (negative control)	-425.5	219.5	11	control	One-Way ANOVA
Cav2.1/2.3 II-III loop CT	-470.5	112.6	8	P=0.9849 (n.s.)	Dunnett's Test
Cav2.1/2.3 II-III loop	-958.1	331.3	11	p<0.0001 (****)	
Cav2.1/2.3 CT	-557.7	198.9	9	P=0.5723 (n.s.)	
IV fit: Half-maximal activation voltage V_m (mV)					

$Ca_V2.1$ FT (control)	-19.75	3.212	11	control	
$Ca_V2.1^{-/-}$/ $Cav2.2^{-/-}$	-12.38	5.791	11	p=0.0392 (*)	One-Way ANOVA
Cav2.1/2.3 II-III loop CT	-17.62	8.814	8	p=0.8972 (n.s.)	Dunnett's Test
Cav2.1/2.3 II-III loop	-15.52	7.123	11	p=0.3787 (n.s.)	
Cav2.1/2.3 CT	-12.85	7.367	9	p=0.0780 (n.s.)	
IV fit: Voltage-dependence of activation K_m (mV)					
$Ca_V2.1$ FT (control)	2.854	1.673	11	control	One-Way ANOVA
$Ca_V2.1^{-/-}$/ $Cav2.2^{-/-}$	8.123	0.7658	11	p=0.0002 (***)	Dunnett's test
Cav2.1/2.3 II-III loop CT	10.48	4.514	8	p<0.0001 (****)	
Cav2.1/2.3 II-III loop	3.622	1.148	11	p=0.9159 (n.s.)	
Cav2.1/2.3 CT	7.886	3.293	9	p=0.0007 (***)	
Boltzmann fit: Half-maximal activation voltage $V_{0.5}$ (mV)					
$Ca_V2.1$ FT (control)	-17.29	4.761	11	control	One-Way ANOVA
$Ca_V2.1^{-/-}$/ $Cav2.2^{-/-}$	-14.82	5.428	11	p=0.7135 (n.s.)	Dunnett's test
Cav2.1/2.3 II-III loop CT	-11.25	6.953	8	p=0.0924 (n.s.)	One-Way ANOVA
Cav2.1/2.3 II-III loop	-14.25	5.943	11	p=0.5513 (n.s.)	Dunnett's test
Cav2.1/2.3 CT	-11.34	5.750	9	p=0.0841 (n.s.)	
Boltzmann fit: Voltage-dependence K (mV)					
$Ca_V2.1$ FT (control)	5.052	5.07	11	positive control	
$Ca_V2.1^{-/-}$/ $Cav2.2^{-/-}$	5.756	2.624	11	p=0.9880 (n.s.)	One-Way ANOVA
Cav2.1/2.3 II-III loop CT	6.670	4.116	8	p=0.8508 (n.s.)	Dunnett's test
Cav2.1/2.3 II-III loop	6.628	4.506	11	p=0.8231 (n.s.)	
Cav2.1/2.3 CT	7.556	5.261	9	p=0.5365 (n.s.)	

Table4. Agatoxin sensitive fraction.

Parameter	Mean	SD	n	P	statistics
Agatoxin sensitive fraction (%)					
$Ca_V2.1$ FT	89.5	4.95	3	control	One-Way ANOVA
Cav2.1/2.3 II-III loop CT	67.67	7.371	3	p=0.0111 (*)	
Cav2.1/2.3 II-III loop	93	1.414	4	p=0.8282 (n.s.)	Dunnett's Test
Cav2.1/2.3 CT	86.33	9.074	3	p=0.8787 (n.s.)	

766 **Table5. Electrophysiological parameters of IV relations of Ca^{2+} currents.**
767

Parameter	Mean	SD	n	P	statistics
Max. Ca^{2+} current amplitude I_{max} (pA)					
$Ca_V2.1$ FT	-1222	256.2	11	control	
$Ca_V2.1$ Δ2016	-1241	207.4	6	p=0.8827 (n.s.)	Unpaired t test
$Ca_V2.1$ Δ2016	-1241	207.4	6	Positive control	
Cav2.1/2.3 CT2016-2368	-934.1	210.6	12	p=0.0209 (*)	One-Way ANOVA
Cav2.1/2.3 CT1967-2368	-839.5	251.9	8	p=0.0047 (**)	Dunnett's Test
Cav2.1/2.3 CT1933-2368	-557.7	198.9	9	P<0.0001 (****)	
$Ca_V2.1$ delta 2016	-1241	207.4	6	P<0.0001 (****)	
Cav2.1/2.3 CT 2016-2368	-934.1	210.6	12	p=0.0013 (**)	One-Way ANOVA
Cav2.1/2.3 CT 1967-2368	-839.5	251.9	8	P=0.0321 (*)	Dunnett's Test
Cav2.1/2.3 CT 1933-2368	-557.7	198.9	9	Negative control	

768
769 **Table6. Electrophysiological parameters of IV relations of Ca^{2+} currents.**
770

Parameter	Mean	SD	n	P	statistics
Max. Ca^{2+} current amplitude I_{max} (pA)					
$Ca_V2.1$ FT	-1222	256.2	11	control	One-Way ANOVA
$Ca_V2.1/2.2$ CT	-1049	479.4	11	p=0.3885 (n.s.)	Dunnett's Test
$Ca_V2.1^{-/-}$/ $Cav2.2^{-/-}$	-425.5	219.5	11	P<0.0001 (****)	

771
772 **Table7. Electrophysiological parameters of IV relations of Ca^{2+} currents.**
773

Parameter	Mean	SD	n	P	statistics
Max. Ca^{2+} current amplitude I_{max} (pA)					
Pun $Ca_V2.1$ FT	-1438	263.9	7	control	One-Way ANOVA
Pun $Ca_V2.1/2.2$ CT	-1534	370.4	9	p=0.7617 (n.s.)	Dunnett's Test
Pun $Ca_V2.1/2.3$ CT	-772.8	291.8	10	P=0.0006 (***)	
Pun $Ca_V2.1$ FT	-1438	263.9	7	P<0.0001 (****)	One-Way ANOVA
Pun $Ca_V2.1/2.3$ CT	-772.8	291.8	10	p=0.1816 (n.s.)	Dunnett's Test
Syn $Ca_V2.1/2.3$ CT	-557.7	198.9	9	Negative control	

774
775 **Table8. Capacitances of calyx of Held expressing Ca_V2 hybrid channels.**
776

Parameter	Mean	SD	n	P	statistics
Membrane capacitance C_{slow} (pF)					
Wildtype (control)	20.59	4.220	10	p=0.9246 (n.s.)	

$Ca_V2.1$ FT	23.80	5.150	11	control	
$Ca_V2.1^{-/-}$/ $Cav2.2^{-/-}$	22.85	8.831	11	p=0.9996 (n.s.)	
Cav2.1/2.3 II-III loop CT	21.72	6.096	8	p=0.9990 (n.s.)	
Cav2.1/2.3 II-III loop	25.76	6.045	11	p=0.9960 (n.s.)	One-Way ANOVA
Cav2.1/2.3 CT	19.06	4.894	9	p=0.6135 (n.s.)	Dunnett's Test
$Ca_V2.1$ Δ2016	27.26	3.420	6	p=0.9522 (n.s.)	
Cav2.1/2.3 CT 2016-2368	28.22	7.622	12	p=0.6103 (n.s.)	
Cav2.1/2.3 CT 1967-2368	27.47	8.513	9	p=0.8646 (n.s.)	
Cav2.1/2.2 CT	21.94	9.095	11	p=0.9991 (n.s.)	
Pun $Ca_V2.1$ FT	21.44	5.828	7	p=0.9955 (n.s.)	
Pun $Ca_V2.1$/2.2 CT	23.94	4.943	9	p>0.9999 (n.s.)	
Pun $Ca_V2.1$/2.3 CT	26.04	7.309	10	p=0.9916 (n.s.)	

780
781 **References**

782 Bewig B & Schmidt WE. (2000). Accelerated titering of adenoviruses. *Biotechniques* **28,** 870-
783 873.

784
785 Chaudhuri D, Chang SY, DeMaria CD, Alvania RS, Soong TW & Yue DT. (2004). Alternative
786 splicing as a molecular switch for Ca^{2+}/calmodulin-dependent facilitation of P/Q-type
787 Ca^{2+} channels. *J Neurosci* **24,** 6334-6342.

788
789 Chen ZX, Cooper B, Kalla S, Varoqueaux F & Young SM. (2013). The Munc13 Proteins
790 Differentially Regulate Readily Releasable Pool Dynamics and Calcium-Dependent
791 Recovery at a Central Synapse. *Journal of Neuroscience* **33,** 8336-8351.

792
793 Cole RL, Lechner SM, Williams ME, Prodanovich P, Bleicher L, Varney MA & Gu G. (2005).
794 Differential distribution of voltage-gated calcium channel alpha-2 delta (alpha2delta)
795 subunit mRNA-containing cells in the rat central nervous system and the dorsal root
796 ganglia. *J Comp Neurol* **491,** 246-269.

797
798 De Waard M, Pragnell M & Campbell KP. (1994). Ca2+ channel regulation by a conserved beta
799 subunit domain. *Neuron* **13,** 495-503.

800
801 Dolphin AC. (2012). Calcium channel auxiliary alpha2delta and beta subunits: trafficking and
802 one step beyond. *Nat Rev Neurosci* **13,** 542-555.

803
804 Dolphin AC & Lee A. (2020). Presynaptic calcium channels: specialized control of synaptic
805 neurotransmitter release. *Nat Rev Neurosci* **21,** 213-229.

806
807 Dong W, Radulovic T, Goral RO, Thomas C, Montesinos MS, Guerrero-Given D, Hagiwara A,
808 Putzke T, Hida Y, Abe M, Sakimura K, Kamasawa N, Ohtsuka T & Young SM. (2018).
809 CAST/ELKS Proteins Control Voltage-Gated Ca2+ Channel Density and Synaptic
810 Release Probability at a Mammalian Central Synapse. *Cell Rep* **24,** 284-+.

811
812 Doughty JM, Barnes-Davies M, Rusznak Z, Harasztosi C & Forsythe ID. (1998). Contrasting
813 Ca2+ channel subtypes at cell bodies and synaptic terminals of rat anterioventral
814 cochlear bushy neurones. *J Physiol* **512 (Pt 2),** 365-376.

815
816 Eggermann E, Bucurenciu I, Goswami SP & Jonas P. (2011). Nanodomain coupling between
817 Ca(2)(+) channels and sensors of exocytosis at fast mammalian synapses. *Nat Rev*
818 *Neurosci* **13,** 7-21.

819
820 Ferron L, Koshti S & Zamponi GW. (2021). The life cycle of voltage-gated Ca(2+) channels in
821 neurons: an update on the trafficking of neuronal calcium channels. *Neuronal Signal* **5,**
822 NS20200095.

Giugovaz-Tropper B, Gonzalez-Inchauspe C, Di Guilmi MN, Urbano FJ, Forsythe ID & Uchitel OD. (2011). P/Q-type calcium channel ablation in a mice glycinergic synapse mediated by multiple types of Ca(2)+ channels alters transmitter release and short term plasticity. *Neuroscience* **192,** 219-230.

Hoppa MB, Lana B, Margas W, Dolphin AC & Ryan TA. (2012). alpha2delta expression sets presynaptic calcium channel abundance and release probability. *Nature* **486,** 122-125.

Inchauspe CG, Martini FJ, Forsythe ID & Uchitel OD. (2004). Functional compensation of P/Q by N-type channels blocks short-term plasticity at the calyx of Held presynaptic terminal. *J Neurosci* **24,** 10379-10383.

Iwasaki S, Momiyama A, Uchitel OD & Takahashi T. (2000). Developmental changes in calcium channel types mediating central synaptic transmission. *J Neurosci* **20,** 59-65.

Iwasaki S & Takahashi T. (1998). Developmental changes in calcium channel types mediating synaptic transmission in rat auditory brainstem. *J Physiol* **509 (Pt 2),** 419-423.

Jun K, Piedras-Renteria ES, Smith SM, Wheeler DB, Lee SB, Lee TG, Chin H, Adams ME, Scheller RH, Tsien RW & Shin HS. (1999). Ablation of P/Q-type Ca(2+) channel currents, altered synaptic transmission, and progressive ataxia in mice lacking the alpha(1A)-subunit. *Proc Natl Acad Sci U S A* **96,** 15245-15250.

Kaja S, Van de Ven RC, Ferrari MD, Frants RR, Van den Maagdenberg AM & Plomp JJ. (2006). Compensatory contribution of Cav2.3 channels to acetylcholine release at the neuromuscular junction of tottering mice. *J Neurophysiol* **95,** 2698-2704.

Kamp MA, Krieger A, Henry M, Hescheler J, Weiergraber M & Schneider T. (2005). Presynaptic 'Ca_V2.3-containing' E-type Ca^{2+} channels share dual roles during neurotransmitter release. *Eur J Neurosci* **21,** 1617-1625.

Kamp MA, Shakeri B, Tevoufouet EE, Krieger A, Henry M, Behnke K, Herzig S, Hescheler J, Radhakrishnan K, Parent L & Schneider T. (2012). The C-terminus of human Ca_V2.3 voltage-gated calcium channel interacts with alternatively spliced calmodulin-2 expressed in two human cell lines. *Biochim Biophys Acta* **1824,** 1045-1057.

Lee A, Zhou H, Scheuer T & Catterall WA. (2003). Molecular determinants of Ca(2+)/calmodulin-dependent regulation of Ca(v)2.1 channels. *Proc Natl Acad Sci U S A* **100,** 16059-16064.

Lubbert M, Goral RO, Keine C, Thomas C, Guerrero-Given D, Putzke T, Satterfield R, Kamasawa N & Young SM, Jr. (2019). Ca(V)2.1 alpha(1) Subunit Expression Regulates

866 Presynaptic Ca(V)2.1 Abundance and Synaptic Strength at a Central Synapse. *Neuron*
867 **101,** 260-273 e266.

868

869 Lubbert M, Goral RO, Satterfield R, Putzke T, van den Maagdenberg AM, Kamasawa N &
870 Young SM, Jr. (2017). A novel region in the Ca(V)2.1 alpha(1) subunit C-terminus
871 regulates fast synaptic vesicle fusion and vesicle docking at the mammalian presynaptic
872 active zone. *Elife* **6**.

873

874 Mochida S, Few AP, Scheuer T & Catterall WA. (2008). Regulation of presynaptic Ca(V)2.1
875 channels by Ca2+ sensor proteins mediates short-term synaptic plasticity. *Neuron* **57,**
876 210-216.

877

878 Mochida S, Westenbroek RE, Yokoyama CT, Zhong H, Myers SJ, Scheuer T, Itoh K & Catterall
879 WA. (2003). Requirement for the synaptic protein interaction site for reconstitution of
880 synaptic transmission by P/Q-type calcium channels. *Proc Natl Acad Sci U S A* **100,**
881 2819-2824.

882

883 Montesinos MS, Chen ZX & Young SM. (2011). pUNISHER: a high-level expression cassette
884 for use with recombinant viral vectors for rapid and long term in vivo neuronal expression
885 in the CNS. *J Neurophysiol* **106,** 3230-3244.

886

887 Montesinos MS, Satterfield R & Young SM, Jr. (2016). Helper-Dependent Adenoviral Vectors
888 and Their Use for Neuroscience Applications. *Methods Mol Biol* **1474,** 73-90.

889

890 Mori MX, Vander Kooi CW, Leahy DJ & Yue DT. (2008). Crystal structure of the CaV2 IQ
891 domain in complex with Ca2+/calmodulin: high-resolution mechanistic implications for
892 channel regulation by Ca2+. *Structure* **16,** 607-620.

893

894 Muller CS, Haupt A, Bildl W, Schindler J, Knaus HG, Meissner M, Rammner B, Striessnig J,
895 Flockerzi V, Fakler B & Schulte U. (2010). Quantitative proteomics of the Cav2 channel
896 nano-environments in the mammalian brain. *Proc Natl Acad Sci U S A* **107,** 14950-
897 14957.

898

899 Nanou E & Catterall WA. (2018). Calcium Channels, Synaptic Plasticity, and Neuropsychiatric
900 Disease. *Neuron* **98,** 466-481.

901

902 Nanou E, Yan J, Whitehead NP, Kim MJ, Froehner SC, Scheuer T & Catterall WA. (2016).
903 Altered short-term synaptic plasticity and reduced muscle strength in mice with impaired
904 regulation of presynaptic CaV2.1 Ca2+ channels. *Proc Natl Acad Sci U S A* **113,** 1068-
905 1073.

906

907 Palmer DJ & Ng P. (2005). Helper-dependent adenoviral vectors for gene therapy. *Hum Gene*
908 *Ther* **16,** 1-16.

909

910 Pilch KS, Ramgoolam KH & Dolphin AC. (2022). Involvement of Ca(V) 2.2 channels and
911 alpha(2) delta-1 in homeostatic synaptic plasticity in cultured hippocampal neurons. *J*
912 *Physiol* **600,** 5333-5351.

913

914 Radulovic T, Dong W, Goral RO, Thomas CI, Veeraraghavan P, Montesinos MS, Guerrero-
915 Given D, Goff K, Lubbert M, Kamasawa N, Ohtsuka T & Young SM. (2020). Presynaptic
916 development is controlled by the core active zone proteins CAST/ELKS. *J Physiol-*
917 *London* **598,** 2431-2452.

918

919 Rajapaksha WR, Wang D, Davies JN, Chen L, Zamponi GW & Fisher TE. (2008). Novel splice
920 variants of rat CaV2.1 that lack much of the synaptic protein interaction site are
921 expressed in neuroendocrine cells. *J Biol Chem* **283,** 15997-16003.

922

923 Rothman JS & Silver RA. (2018). NeuroMatic: An Integrated Open-Source Software Toolkit for
924 Acquisition, Analysis and Simulation of Electrophysiological Data. *Front Neuroinform* **12,**
925 14.

926

927 Serra SA, Gene GG, Elorza-Vidal X & Fernandez-Fernandez JM. (2018). Cross talk between
928 beta subunits, intracellular Ca(2+) signaling, and SNAREs in the modulation of Ca(V) 2.1
929 channel steady-state inactivation. *Physiol Rep* **6**.

930

931 Simms BAZ, G. W. (2014). Neuronal voltage-gated calcium channels: structure, function, and
932 dysfunction. *Neuron* **82,** 24-45.

933

934 Stephani F, Scheuer V, Eckrich T, Blum K, Wang W, Obermair GJ & Engel J. (2019). Deletion
935 of the Ca(2+) Channel Subunit alpha(2)delta3 Differentially Affects Ca(v)2.1 and
936 Ca(v)2.2 Currents in Cultured Spiral Ganglion Neurons Before and After the Onset of
937 Hearing. *Front Cell Neurosci* **13,** 278.

938

939 Szabo Z, Obermair GJ, Cooper CB, Zamponi GW & Flucher BE. (2006). Role of the synprint
940 site in presynaptic targeting of the calcium channel CaV2.2 in hippocampal neurons. *Eur*
941 *J Neurosci* **24,** 709-718.

942

943 Voigt A, Freund R, Heck J, Missler M, Obermair GJ, Thomas U & Heine M. (2016). Dynamic
944 association of calcium channel subunits at the cellular membrane. *Neurophotonics* **3,**
945 041809.

946

947 Weiss N & Zamponi GW. (2017). Trafficking of neuronal calcium channels. *Neuronal Signal* **1,**
948 NS20160003.

949

950 Wiser O, Cohen R & Atlas D. (2002). Ionic dependence of Ca2+ channel modulation by syntaxin
951 1A. *Proc Natl Acad Sci U S A* **99,** 3968-3973.

952

953 Xie M, Li X, Han J, Vogt DL, Wittemann S, Mark MD & Herlitze S. (2007). Facilitation versus
954 depression in cultured hippocampal neurons determined by targeting of Ca2+ channel
955 Cavbeta4 versus Cavbeta2 subunits to synaptic terminals. *J Cell Biol* **178,** 489-502.

956

957 Yokoyama CT, Myers SJ, Fu J, Mockus SM, Scheuer T & Catterall WA. (2005). Mechanism of
958 SNARE protein binding and regulation of Cav2 channels by phosphorylation of the
959 synaptic protein interaction site. *Mol Cell Neurosci* **28,** 1-17.

960

961 Young SM, Jr. & Neher E. (2009). Synaptotagmin has an essential function in synaptic vesicle
962 positioning for synchronous release in addition to its role as a calcium sensor. *Neuron*
963 **63,** 482-496.

964

965 Young SM, Jr. & Veeraraghavan P. (2021). Presynaptic voltage-gated calcium channels in the
966 auditory brainstem. *Mol Cell Neurosci* **112,** 103609.

967

968 Zhong H, Yokoyama CT, Scheuer T & Catterall WA. (1999). Reciprocal regulation of P/Q-type
969 Ca2+ channels by SNAP-25, syntaxin and synaptotagmin. *Nat Neurosci* **2,** 939-941.

970

971

972

973

974

975 **Additional information section**

976 **Conflict of Interest –** the authors report no conflict of interest.

977 **Author contributions:** J.L. and P.V., carried out experiments and analyzed data. S.M.Y, Jr
978 developed the mouse model S.M.Y, Jr planned the project and analyzed data. J.L. and S.M.Y, Jr.
979 wrote the manuscript. All authors jointly revised the paper. All authors approved the final version
980 of the manuscript, agree to be accountable for all aspects of the work in ensuring that questions
981 related to the accuracy or integrity of any part of the work are appropriately investigated and
982 resolved, all persons designated as authors qualify for authorship, and all those who qualify for
983 authorship are listed.

984 **Funding sources**: This work was supported by the National Institutes of Deafness and
985 Communication Disorders (R01 DC014093), the National Institute of Neurological Disorders and
986 Stroke (R01 NS110742), and the National Center for Advancing Translational Sciences.
987 R03TR004161-01 and the University of Iowa Distinguished Scholar Award. (S.M.Y., Jr) and the
988 American Heart Association (Predoctoral fellowship 23PRE1019152) (J. L)

989 **Acknowledgements**: We thank members of the Young lab for their comments and critiques of
990 the manuscript and project. We thank Hao Li for help with for HdAd viral vector production. We
991 thank Dr. Susan Stamnes and University of Iowa viral vector core, for help with HdAd vector
992 production and tittering. We thank Dr. Phillip Ng and Dr. Brendan Lee for gifts of HdAd packing
993 plasmids and HdAd stuffer DNA, respectively.

994

995

996

997

998

999

1000

1001

1002

1003

1004

1005

1006

1007 .

Fig. 1

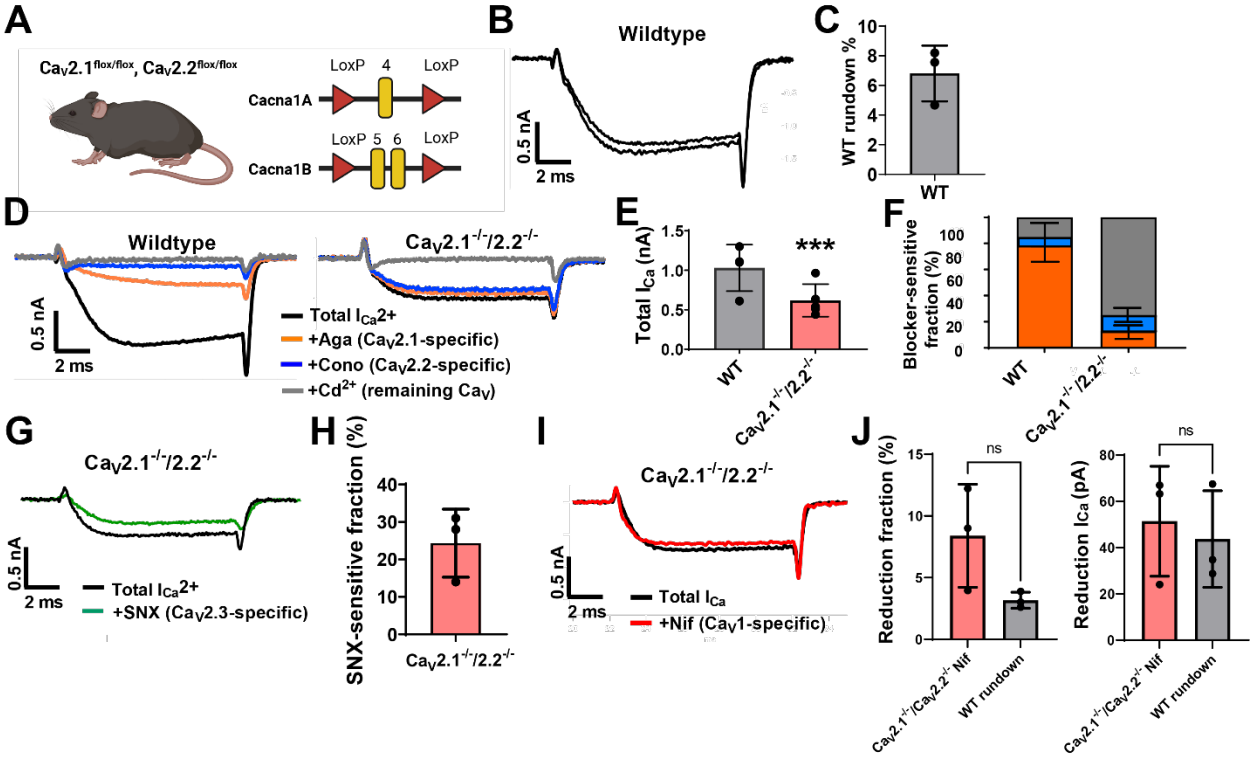

1008

1009

1010

Fig. 2

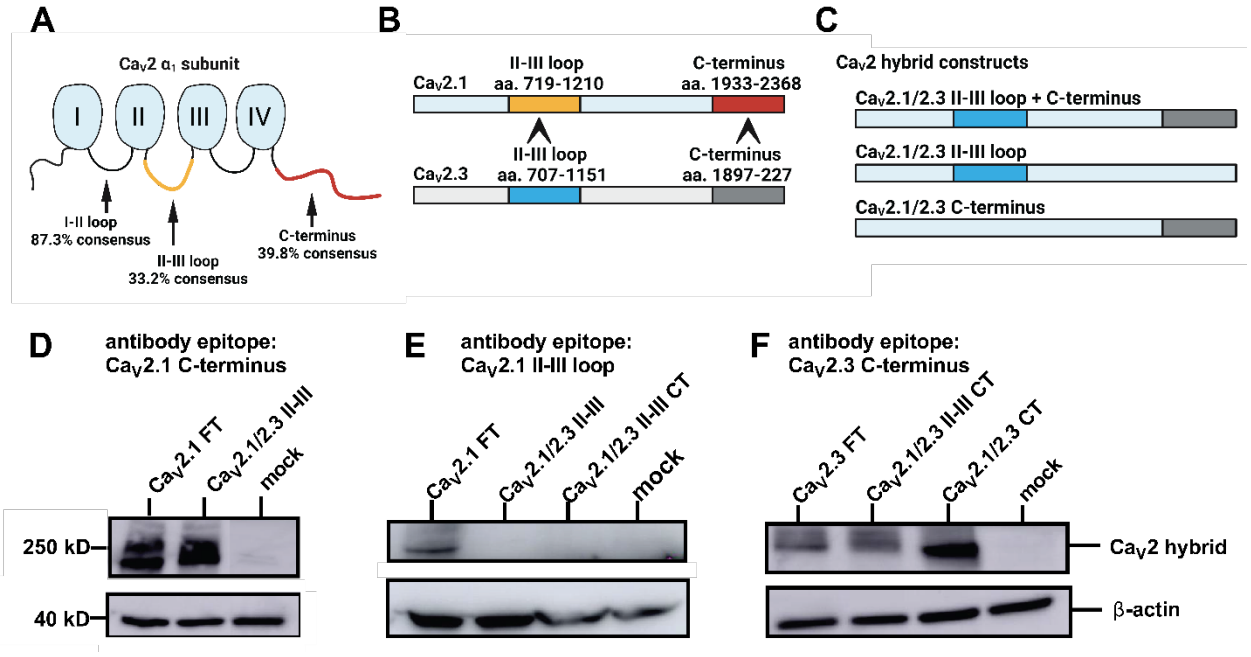

1011

1012

1013

Fig. 3

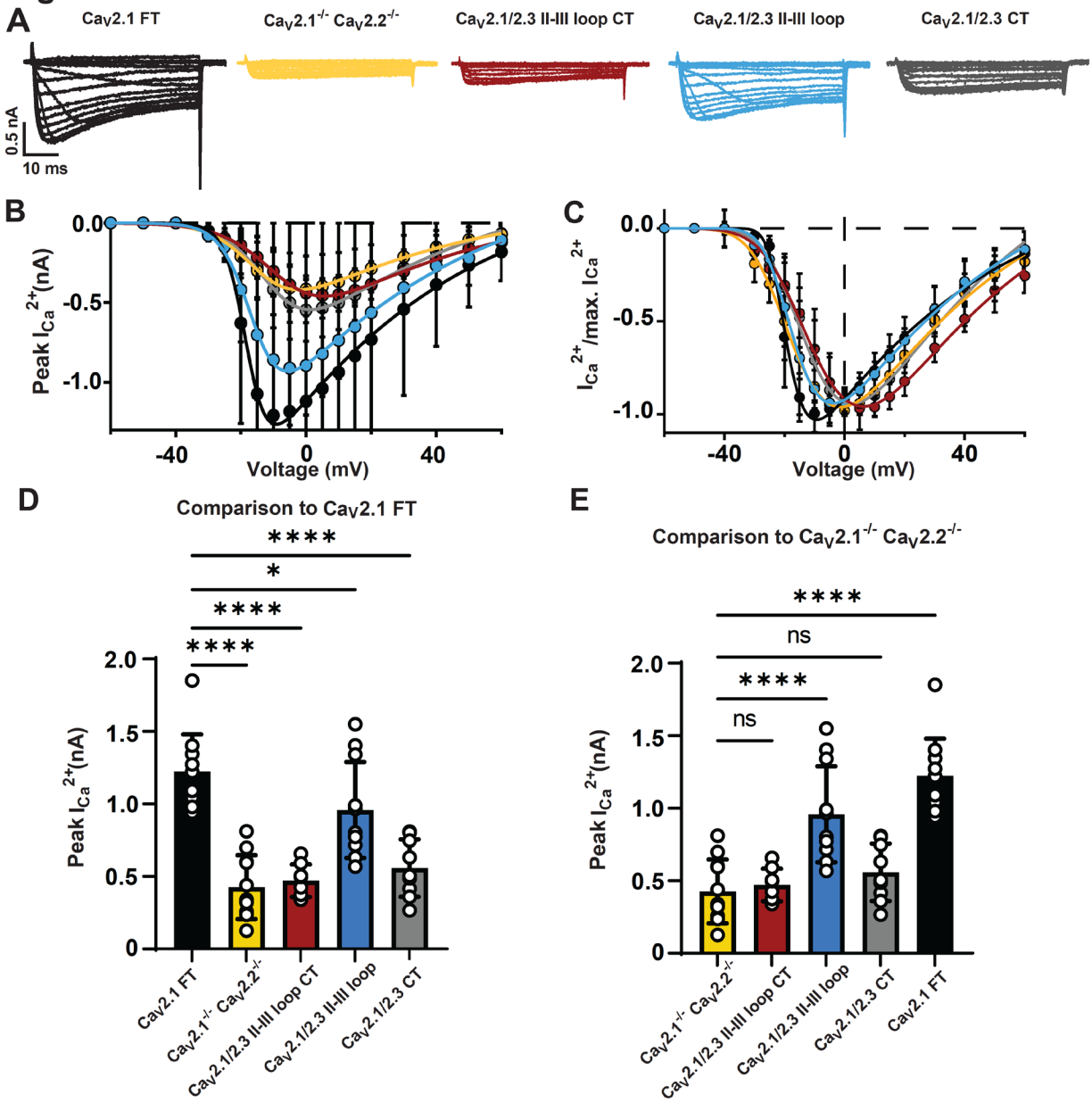
A
CaV2.1 FT
CaV2.1-/- CaV2.2-/-
CaV2.1/2.3 II-III loop CT
CaV2.1/2.3 II-III loop
CaV2.1/2.3 CT
0.5 nA
10 ms
B
Peak ICa2+(nA)
Voltage (mV)
C
ICa2+/max. ICa2+
Voltage (mV)
D
Comparison to CaV2.1 FT
****
*
****
****
Peak ICa2+(nA)
CaV2.1 FT
CaV2.1-/- CaV2.2-/-
CaV2.1/2.3 II-III loop CT
CaV2.1/2.3 II-III loop
CaV2.1/2.3 CT
E
Comparison to CaV2.1-/- CaV2.2-/-
****
ns
****
ns
Peak ICa2+(nA)
CaV2.1-/- CaV2.2-/-
CaV2.1/2.3 II-III loop CT
CaV2.1/2.3 II-III loop
CaV2.1/2.3 CT
CaV2.1 FT

1014

Fig. 4

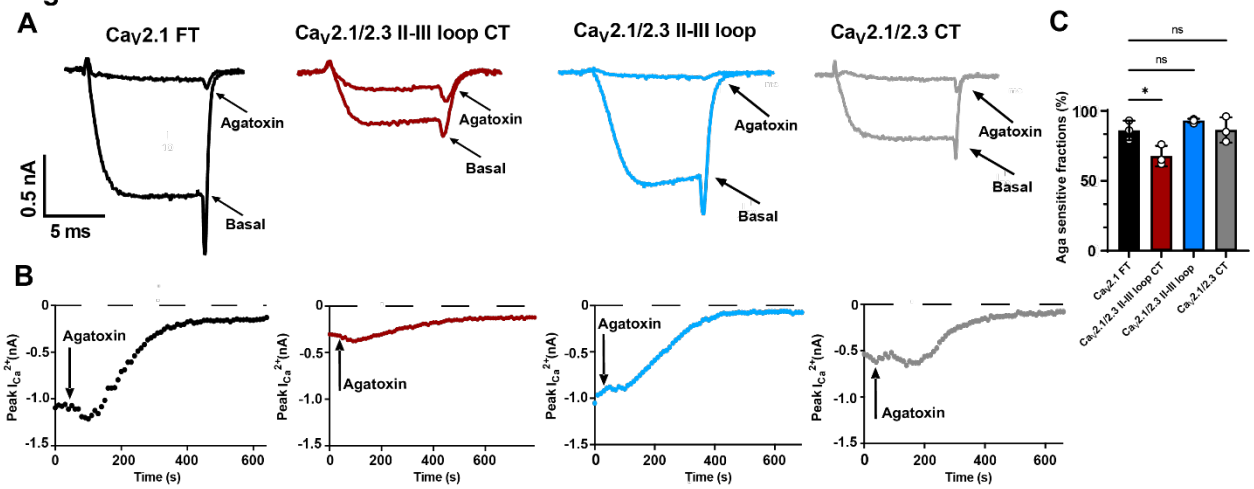

1015

1016

Fig. 5

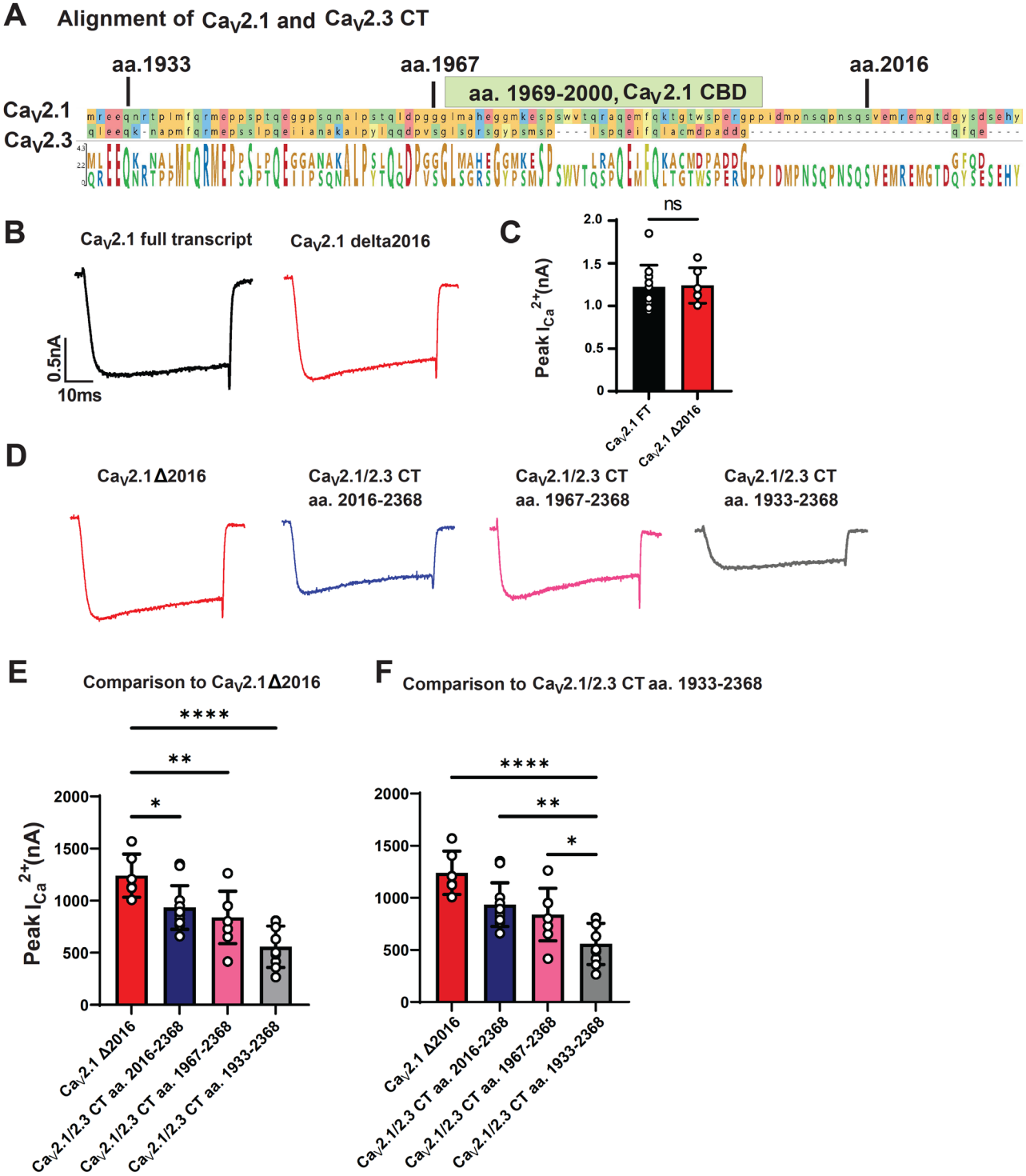
A
Alignment of CaV2.1 and CaV2.3 CT
aa.1933
aa.1967
aa.2016
aa. 1969-2000, CaV2.1 CBD
CaV2.1
CaV2.3
B
CaV2.1 full transcript
CaV2.1 delta2016
0.5nA
10ms
C
ns
Peak ICa2+(nA)
CaV2.1 FT
CaV2.1 Δ2016
D
CaV2.1Δ2016
CaV2.1/2.3 CT aa. 2016-2368
CaV2.1/2.3 CT aa. 1967-2368
CaV2.1/2.3 CT aa. 1933-2368
E
Comparison to CaV2.1Δ2016
F
Comparison to CaV2.1/2.3 CT aa. 1933-2368
Peak ICa2+(nA)
CaV2.1 Δ2016
CaV2.1/2.3 CT aa. 2016-2368
CaV2.1/2.3 CT aa. 1967-2368
CaV2.1/2.3 CT aa. 1933-2368

1017

Fig. 6

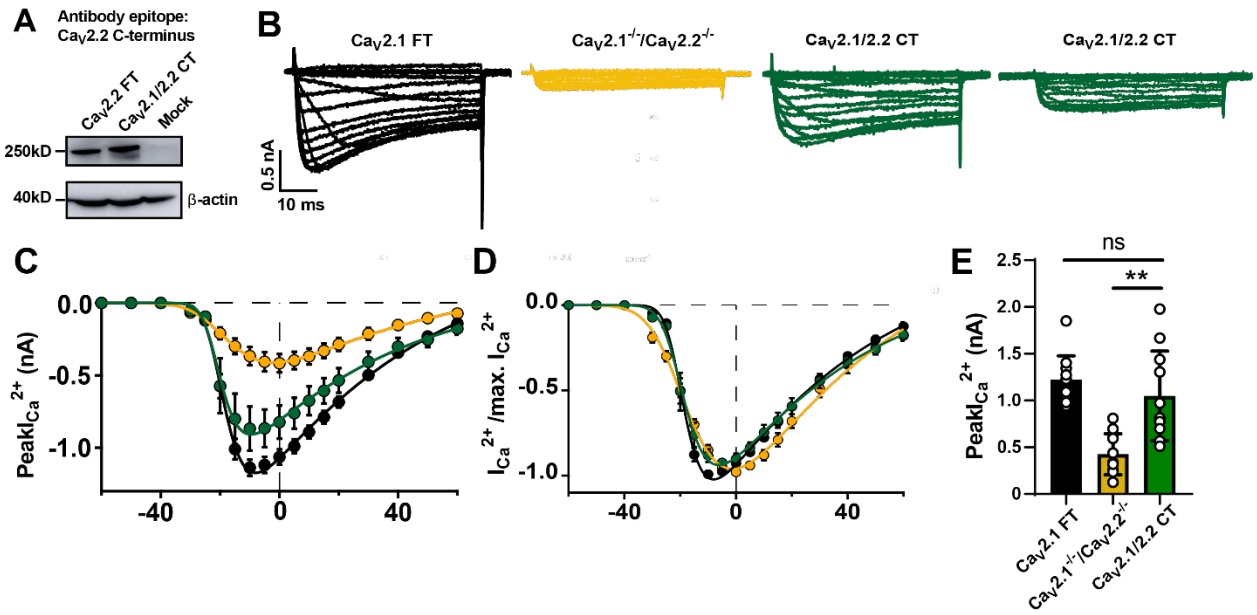

1018

1019

Fig. 7

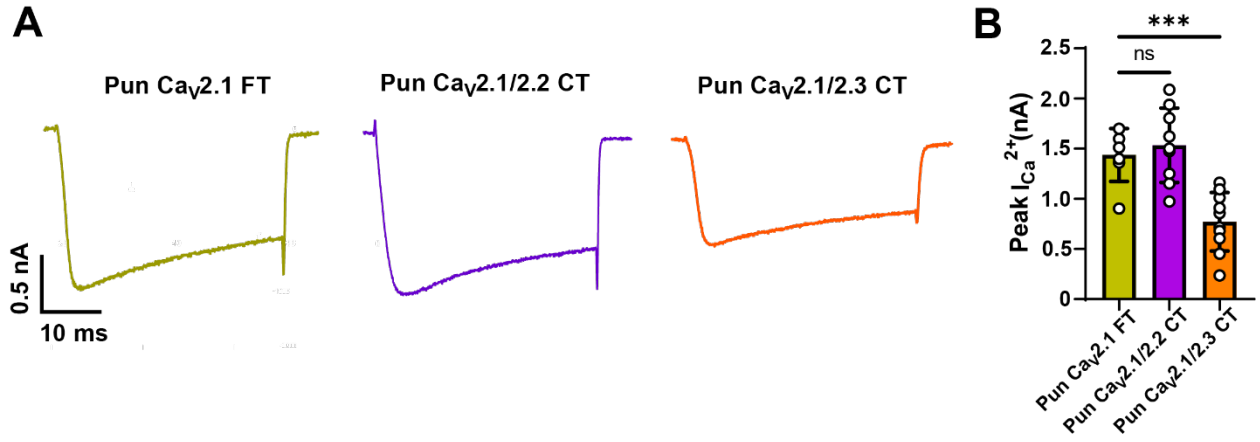
A
Pun CaV2.1 FT
Pun CaV2.1/2.2 CT
Pun CaV2.1/2.3 CT
0.5 nA
10 ms
B
***
ns
Peak ICa2+(nA)
2.5
2.0
1.5
1.0
0.5
0
Pun CaV2.1 FT
Pun CaV2.1/2.2 CT
Pun CaV2.1/2.3 CT

1020